Report Title:

TOXIC SUBSTANCES FROM COAL COMBUSTION -- A COMPREHENSIVE ASSESSMENT

Report Type: QUARTERLY

Reporting Period Start Date: 08/01/1997 End Date: 06/30/1998

Principal Author(s): C.L.Senior,T.Panagiotou[1],J.O.L.Wendt,W.Seames[2]
F.E. Huggins, G.P. Huffman, N. Yap(3)
M.R.Ames,I.Olmez,T.Zeng(4),A.F.Sarofim(5)
A.Kolker,R.Finkelman(6)
J.J.Helble(7)

Report Issue Date: 07/16/1998

DOE Award No.: DE- AC22 -95PC95101

Submitting Organization(s)

Name & Address

[1]Physical Sciences Inc.
20 New England Business Center
Andover, MA 01810-1077
[2]University of Arizona
Tucson, AZ 85721

(1)

(3) University of Kentucky
Lexington, KY 40506-0059

(2)

(4)Massachusetts Institute of Technology
Cambridge, MA 02139
(5)University of Utah
Salt Lake City, UT 84112

(3)

(6) U.S. Geological Survey
Reston, VA 22092

(4)

(7) University of Connecticut
Storrs, CT 06269

(5)

DISCLAIMER

DISCLAIMER

Portions of this document may be illegible in electronic image products. Images are produced from the best available original document.

ABSTRACT

The Clean Air Act Amendments of 1990 identify a number of hazardous air pollutants (HAPs) as candidates for regulation. Should regulations be imposed on HAP emissions from coal-fired power plants, a sound understanding of the fundamental principles controlling the formation and partitioning of toxic species during coal combustion will be needed. With support from the Federal Energy Technology Center (FETC), the Electric Power Research Institute, and VTT (Finland), Physical Sciences Inc. (PSI) has teamed with researchers from USGS, the Massachusetts Institute of Technology (MIT), the University of Arizona (UA), the University of Kentucky (UK), the University of Connecticut (UC), the University of Utah (UU) and the University of North Dakota Energy & Environmental Research Center (EERC) to develop a broadly applicable emissions model useful to regulators and utility planners. The new Toxics Partitioning Engineering Model (ToPEM) will be applicable to *all* combustion conditions including new fuels and coal blends, low-NO_x combustion systems, and new power generation plants. Development of ToPEM will be based on PSI's existing Engineering Model for Ash Formation (EMAF). This report covers the reporting period from the submission of the draft Phase I Final Report through the end of June, 1998. During this period two of the three Phase II coals were procured and pulverized samples were distributed to team members. Analysis of Phase I X-Ray Absorption Fine Structure (XAFS) data, particularly of mercury in sorbent samples, continued. An improved method for identifying mercury compounds on sorbents was developed, leading to a clearer understanding of forms of mercury in char and sorbents exposed to flue gas. Additional analysis of Phase I large scale combustion data was performed to investigate mechanistic information related to the fate of the radionuclides Cs, Th, and Co. Modeling work for this period was focused on building and testing a sub-model for vaporization of major elements during combustion.

TABLE OF CONTENTS

LIST OF GRAPHICAL MATERIALS

LIST OF GRAPHICAL MATERIALS (Continued)

LIST OF GRAPHICAL MATERIALS (Continued)

LIST OF GRAPHICAL MATERIALS (Continued)

LIST OF TABLES

SECTION 1

EXECUTIVE SUMMARY

1. EXECUTIVE SUMMARY

The technical objectives of this project are:

a) To identify the effect of the mode-of-occurrence of toxic elements in coal on the partitioning of these elements among vapor, submicron fume, and fly ash during the combustion of pulverized coal,

b) To identify the mechanisms governing the post-vaporization interaction of toxic elements and major minerals or unburnt char,

c) To determine the effect of combustion environment (i.e., fuel rich or fuel lean) on the partitioning of trace elements between vapor, submicron fume, and fly ash during the combustion of pulverized coal,

d) To model the partitioning of toxic elements between various chemical species in the vapor phase and between the vapor phase and complex aluminosilicate melts,

e) To develop the new Toxics Partitioning Engineering Model (ToPEM), applicable to *all* combustion conditions including new fuels and coal blends, low-NO_x combustion systems, and new power generation plants.

A description of the work plan for accomplishing these objectives is presented in Section 2.1 of this report.

The work discussed in this report covers the reporting period from the submission of the draft Phase I Final Report through the end of June, 1998. Three coals were selected for detailed study in Phase II: an Ohio bituminous coal, a Wyodak seam Powder River Basin sub-bituminous coal, and a North Dakota lignite. Samples of all three coals were procured. Pulverized samples of two of the coals (Ohio and North Dakota) were distributed to team members. Analytical work on the pulverized samples was started.

Analysis of data taken in the Phase I program continued during the reporting period. Experiments were carried out on the volatility of trace elements during heating of the coals. Relatively slow heating in air (consistent with ASTM ashing procedure, for example) did not produce a significant loss of trace elements in coal samples. However, rapid heating (consistent with the ASTM procedure for determination of volatile matter) resulted in significant loss of trace elements. Further investigations will be undertaken in Phase II to determine if this latter procedure can provide any information on the forms of trace elements in coal samples.

Mass balance closure calculations were made for the combustion experiments at Massachusetts Institute of Technology's (MIT's) Drop Tube Furnace (DTF) and Physical Sciences Inc.'s (PSI's) Entrained Flow Reactor (EFR). In the pyrolysis experiments at MIT, Na and Se showed poor mass balance closure, while in combustion experiments, Na, Cr, Co, and Sb showed poor mass balance closure. The PSI combustion experiments showed low mass balance

closure for Br, As, Se, and Sb. These elements which exhibited poor mass balance closure are either volatile at combustion temperatures or organically associated. Care must be taken in the Phase II combustion experiments at Utah to obtain good mass balance closure for trace elements.

Additional statistical analysis of Phase I data was performed to investigate mechanistic information related to the fate of the radionuclides Cs, Th, and Co during the combustion of Pittsburgh seam coal and Illinois #6 coal at the University of Arizona (UA). Condensation via heterogeneous reaction appears to be the dominant transformation mechanism in the post-combustion zone for all three elements when burning either coal. There was correlation between ash particle Ca concentration and the concentration of Cs and Th when burning Pittsburgh coal, suggesting formation of a calcium-radionuclide complex in the ash. This was not observed for the Illinois coal, nor for Co in either coal. Analytical methods were developed to analyze trace metals on impactor substrates using graphite furnace atomic spectroscopy (GFAA). These methods were applied to additional Phase I test data to determine the concentration of As in Pittsburgh fly ash samples.

During the course of this project (Phase I through the present), we have accumulated much X-Ray Absorption Fine Structure (XAFS) data on mercury in various sorbents and on a wide range of Hg compounds. Almost without exception, the first features that occur on the mercury absorption edge are two inflection points, whose positions and intensities appear to be related to chemical bonding differences. In particular, the separation of these inflection points appears to correlate with differences in the ionicity of the Hg-NN bond. The more ionic compounds of mercury, such as HgO, mercury sulfate, etc., in which the Hg ion is surrounded by oxygen anions, have large values for the separation of the inflection points, whereas the least ionic species such as Hg iodides and diphenyl mercury have small separations. The data for this inflection point difference (IPD) were assembled for 13 pure mercury compounds. These IPD values were compared to those from previously measured mercury sorbent samples. Many of the UA IPD values are compatible with chloride and/or sulfide as the coordinating ligand around mercury. Other sorbent samples obtained from PSI showed values are outside the chloride/ sulfide range. For several zeolite samples the values were higher, whereas several activated carbon samples had lower values. The IPD values for the zeolite sorbents were compatible with oxidic species, such as the sulfate species. The activated carbon samples, however, may indicate that the principal bonding was between Hg and C, as the IPD values are closest to that of diphenyl mercury. Much work remains to be done in Phase II to determine the limits of confidence of the IPD values, but the method of analysis has the potential for pinpointing specific mercury species on solid samples.

Analysis of the vapor phase mercury-char experiments was modified this period to incorporate new XAFS data on forms of sulfur in the char samples. The basic conclusion remained the same: Elemental mercury appears to react chemically with sulfur in the char, particularly organic sulfur, while for mercury chloride, a physical adsorption process seems to be indicated. The IPD values for the chars, as determined by the University of Kentucky (UK), support this conclusion.

During this period development was begun on a submodel that predicts the vaporization of major metals during coal combustion. The model is based on other existing models, experimental data and correlations of data. The main factors that affect the metal vaporization are: the coal rank, the coal type, the coal particle size, the oxygen content (and therefore the particle temperature) and the metal concentration in the coal. Our model predicts fairly accurately the amounts of ash that vaporize and the submicron ash composition from a variety of bituminous coals. The effect of oxygen concentration and the metal composition of the coal on the ash vaporization are predicted well, but the effect of the coal particle diameter is not predicted accurately. Our model predicts fairly accurately the amounts of ash that vaporize and the submicron ash composition from a variety of low rank coals. Coal particle size had a pronounced effect on the ash vaporization, unlike the case of the bituminous coals.

During the next quarter (July through September, 1998), the rest of the coal samples will be distributed to team members. Standard analyses will be completed for the program coals and advanced analyses will be under way. Preparations will be made for combustion experiments at the University of Connecticut (UC), the University of Utah (UU) and the University of Arizona (UA). Model development work on ash vaporization and submicron aerosol formation will continue.

SECTION 2

INTRODUCTION AND PROGRAM OVERVIEW

2. INTRODUCTION AND PROGRAM OVERVIEW

2.1 Introduction

Before electric utilities can plan or implement emissions minimization strategies for hazardous pollutants, they must have an accurate and site-specific means of predicting emissions in all effluent streams for the broad range of fuels and operating conditions commonly utilized. Development of a broadly applicable emissions model useful to utility planners first requires a sound understanding of the fundamental principles controlling the formation and partitioning of toxic species during coal combustion. PSI and its team members will achieve this objective through the development of an "Engineering Model" that accurately predicts the formation and partitioning of toxic species as a result of coal combustion. The "Toxics Partitioning Engineering Model" (ToPEM) will be applicable to all conditions including new fuels or blends, low-NO_x combustion systems, and new power systems being advanced by DOE in the Combustion 2000 program.

Based on a goal of developing and delivering this ToPEM model, a 5-year research program was proposed. This program is divided into a 2-year Phase I program and a 3-year Phase II program. The objective of the ongoing Phase II program is to develop an experimental and conceptual framework for the behavior of selected trace elements (arsenic, selenium, chromium, and mercury) in combustion systems and incorporate these concepts into a new engineering model. This Phase II objective will be achieved by a team of researchers from USGS, the Massachusetts Institute of Technology (MIT), the University of Arizona (UA), the University of Kentucky (UK), the University of Connecticut (UC), the University of Utah (UU), the University of North Dakota Energy & Environmental Research Center (EERC) and PSI. Model development and commercialization will be carried out by PSI.

2.2 Program Overview

Our general approach to the development of the ToPEM model is to break the process for toxic formation into sub-processes, each of which will be addressed by team members who are experts in the area. Ultimately, this will result in new sub-models which will be added to the existing Engineering Model for Ash Formation (EMAF) to create ToPEM. Table 2-1 describes the work breakdown structure for the Phase II program. Figure 2-1 illustrates the relationship between the elements of the Phase I work breakdown structure and the sub-processes. Each of the areas identified in the figure will be addressed in the Phase II program as described below.

Forms of Occurrence of Trace Elements in Coal

One of the most important questions to be answered in the program as a whole is whether the form of a particular element in the coal affects its form of emission at the end of the process. The answer to this question will determine the shape of the sub-models that must be developed in this program. Thus, a detailed understanding of the forms of individual trace elements in coal

Table 2-1. Task Breakdown

Technical Task	Team Member	Task (WBS) Number
Program management	PSI	1
Coal acquisition, characterization	PSI	2
Coal, ash trace element characterization	PSI	2
Coal (and ash) characterization -- forms of occurrence	UK, USGS	3, 4
Coal, ash trace element characterization and mercury capture and analysis	MIT	5.2
Mechanistic study: dilute bench scale combustion tests plus equilibrium, kinetic modeling	UU	5.1
Large scale tests at 100,000 Btu/h facility	UA	6
Mechanistic study of kinetic rates for gas-phase reactions	UC	10
Mercury-fly ash interactions at bench scale	EERC	11
Fundamental Engineering Model development	PSI	9.1
Inorganic emissions: literature survey and model validation	UC	9.2

provides a foundation for much of the rest of the program. Key issues that will be addressed in Phase II are the specific mineral associations of individual elements and the relationship between trace metal form and "standard" coal analyses.

Because of the importance of elemental form (e.g., sulfate versus silicate mineral) on partitioning, it is critical that coals representing a broad range of elemental forms be examined in this program. In Task 2 we will select and acquire a total of three coals for study in this program. The coals chosen will represent a broad range of elemental forms of occurrence taken from the major coal ranks and commercial coal seams used for pulverized coal power generation in the US. Once selected, fresh coal samples will be acquired and distributed to team members. These samples will be subjected to ultimate, proximate, and ASTM ash analysis. Coal samples will be analyzed for trace element concentrations by Neutron Activation Analysis (NAA) at the MIT Nuclear Reactor Laboratory (Task 5.2).

Advanced analytical techniques such as Mössbauer spectroscopy and Computer-Controlled Scanning Electron Microscopy (CCSEM) will be used by UK (Task 3) to determine the major mineral species present in the program coals and the combustion generated ash. Whole coal samples and density segregated coal samples will be studied. This analysis will provide important insight on the minerals present in the coal, how they interact during the combustion process, and how this interaction may affect the partitioning of toxic elements.

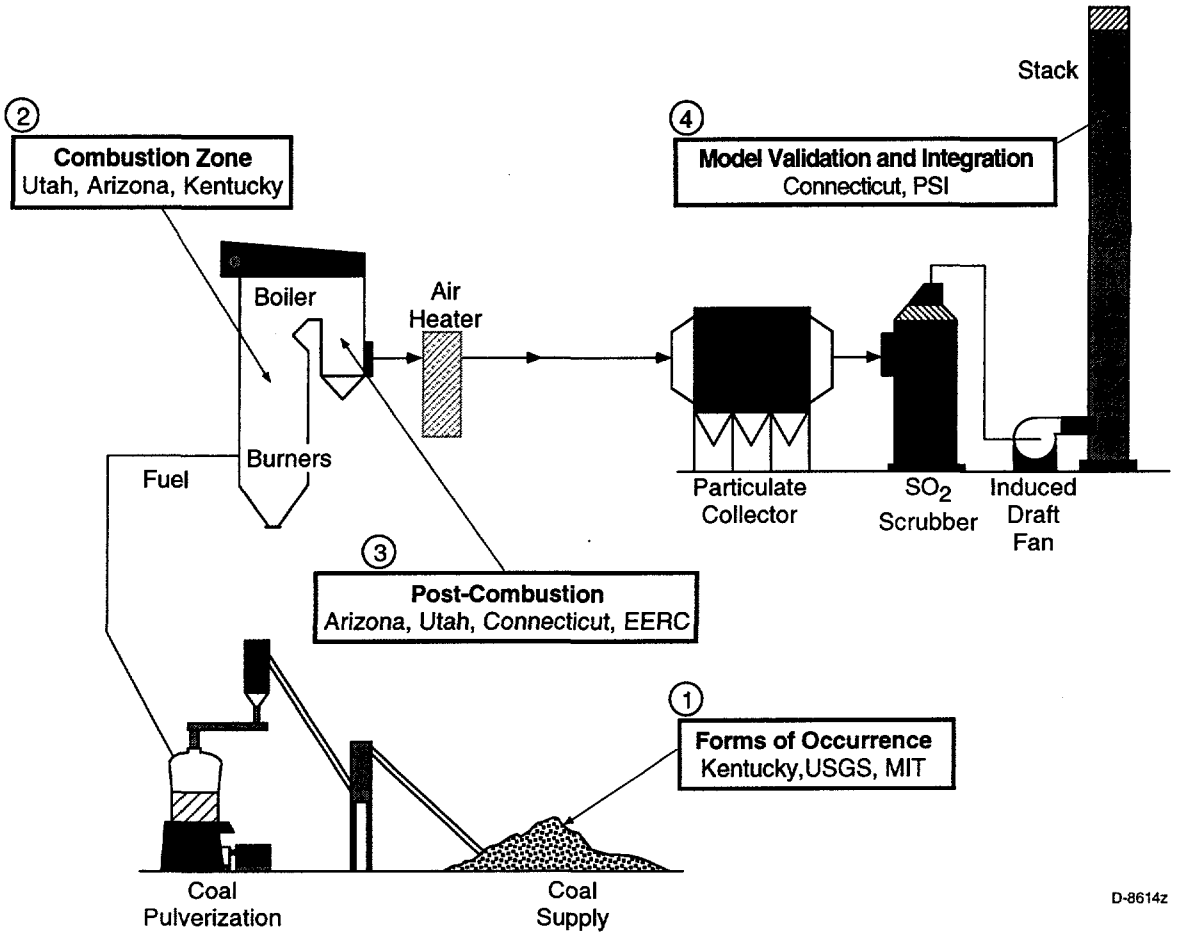

Figure 2-1. Phase II program organization.

Another important issue is the form-of-occurrence of the trace elements in the coal. In this task the mode of occurrence of As, Cr, and Se will be determined by combining XAFS and the Mössbauer/CCSEM derived data discussed above. Hg will also be evaluated where possible. Other less critical trace elements (Mn, Ni, Zn, Pb, U, etc.) may also be evaluated, especially if their abundance is unusually high in any of the program coals. In addition, the form-of-occurrence of Cl and S in coals and chars will be investigated.

As a complement to the XAFS analysis mentioned above, a unique protocol developed by USGS will be used in Task 4 to analyze selected raw coal, and size and density segregated coal, samples for trace element forms of occurrence. This protocol combines low temperature (< 200°C) ashing, chemical analysis, x-ray diffraction, coal segregation via flotation, ammonium acetate and selected acid leaching, electron microbeam measurements, and low and moderate temperature heating tests to determine the forms of elements in coal. Because of the unique combination of existing testing and analytical facilities available at USGS, the work will be conducted at USGS laboratories.

Combustion Zone Transformations

The effect of coal type and combustion conditions on the emission of the toxic trace elements will be investigated using the UU laminar-flow drop tube reactor (Task 5.1). The fundamental mechanisms of toxic species formation and partitioning will be determined from careful examination of the ash formed under a variety of combustion conditions. Measurements will be made of the partitioning of the trace elements in the three coals as a function of temperature and equivalence ratio. These measurements will provide the baseline data on the fraction vaporized. Individual size-segregated ash samples (collected with a cascade impactor) will then be analyzed by NAA for total composition and other analyses as needed, for example, Auger and STEM for surface composition, TEM and SEM for particle morphology, and possibly water washing and/or chemical leaching to determine the solubility of selected trace elements in the ash samples. Samples will also be submitted to UK for chemical species analysis by XAFS and other techniques.

Post-Combustion Transformations

The goal of this task is an increased understanding of the transformations of selected metals as the flue gases cool following the high temperature combustion zone. Bench scale experimentation will be carried out by several organizations as well as large scale combustion measurements. Advanced analytical methods will be used extensively to understand speciation of trace elements in the post-combustion flue gas.

At the UC (Task 10) experiments will focus on determination of trace vapor-ash particle reactions rates in post-combustion gases, including

- Identification of the rate controlling phenomena in the oxidation of arsenic under combustion conditions
- Relative rates of gas-phase reaction of elemental mercury with HCl and Cl_2 under combustion conditions
- Measurement of rates of heterogeneous conversion of HCl to Cl_2 in the presence of coal combustion products such as iron oxide, iron sulfate, and fly ash samples.

Interactions of mercury with ash and ash components at lower temperatures will be the focus of the effort at EERC in Task 11. A bench-scale sorbent evaluation system will be used to increase our understanding of the interactions between gas-phase mercury and coal ash. Experiments will explore the effects of temperature and the interactions between elemental mercury or mercuric chloride and fly ash samples generated under oxidizing conditions, the effect of mercury concentration on the interactions between elemental mercury and fly ash, and the effect of coal combustion conditions on the ash and ultimately on the interaction between mercury and ash.

On a larger scale in Task 6, UA will determine how both coal composition, detailed mineralogy and combustion conditions (including low NO_x conditions) govern the fate of toxic metals under practical time/temperature, self sustained, yet still aerodynamically well defined, pulverized coal combustion conditions. Program coals will be burned in the UA self-sustained combustor under premixed conditions. The baseline tests will employ the naturally occurring temperature profile for each coal at a stoichiometric ratio of 1.2. Samples will be withdrawn at several ports, representing a range of temperatures and residence times. Complete impactor samples will be collected and analyzed for each toxic metal (11 as listed in the CAAA plus U and Th) plus major elements. This will yield the particle size segregated toxic metal composition, which can be compared to data obtained from other tasks of this program. These data will then be examined to determine particle size dependence in order to infer possible mechanisms governing the fate of each metal.

Model Validation

UC will conduct a more in-depth review of the relevant field data on inorganic emissions (Task 9.2). In Phase II we will emphasize use the field data to validate the models we will develop. The Phase II effort focuses on data from the following sources:

- EPRI PISCES
- DOE Program
- VTT (Finland)
- KEMA (Netherlands).

Important issues to be addressed when reviewing these data include mass balance closure, methods of analysis and sample collection, effect of APCD, effect of bulk coal ash chemistry, particle size distribution, and speciation of Hg.

Model Development

In Task 9.1, data obtained from subcontractor and PSI tasks will be combined to create a comprehensive model of the transformations of important inorganic species during combustion. This model, denoted the ToPEM, will be based on an existing model (the PSI Engineering Model for Ash Formation which predicts ash particle size and composition distributions – EMAF). Because the development of this model is strongly dependent on the mechanistic, equilibrium, and kinetic information being developed under the experimental tasks, ToPEM will incorporate information on the mechanisms controlling species behavior, equilibrium modeling where appropriate and kinetic modeling to mimic kinetic constraints on species behavior. During the later stages of the Phase II work, sufficient detailed information will be available to support specific modifications to EMAF in order to describe the combustion transformations of important inorganic trace elements. Based on the experimental studies, equilibrium modeling, and kinetic modeling, it will be clear which modifications are required. Once complete the model will be validated using a combination of laboratory and field data. As part of the validation effort, coal and size fractionated ash samples collected from operating utility boilers will be provided by Dr. Esko Kauppinen of VTT, Finland. Once validated, the ToPEM will be

used to simulate the behavior of these and other coals under utility boiler conditions. The results from these simulations will then be compared to field data from PISCES obtained through EPRI participation in this program, DOE field sampling campaigns, and other relevant data in the literature. This validation procedure will ensure that the model developed as the result of the proposed research efforts accurately predicts the behavior of toxic metals species from a wide range of coals during the combustion process in any combustion system.

SECTION 3

RESULTS AND DISCUSSION

3. RESULTS AND DISCUSSION

3.1 Program Management (PSI)

The Phase II kick-off meeting was held on April 23 at DOE FETC. Representatives from the technical team gave presentations on the highlights of the Phase I program and plans for the Phase II program. The Technical Advisory panel was represented by Bill Linak of US EPA, Ben Pease of ABB, Bob Lisauskas of DB Riley, and Murray Abbott of CONSOL. Paul Chu of EPRI also attended the meeting. Actions and items of note from the kick off meeting are as follows:

- Mike Ames (MIT) will develop a simple mercury sampling method for some of the combustion experiments in the program which will provide speciation information. This will be used at UC, UA, and UU.

- Tom Brown described upcoming field studies which might provide us with data and/or samples to analyze.

- Stan Miller from EERC needs about 100 to 500 g of ash for each coal and/or combustion condition in Task 11. At the UA combustor, the coal feed rate is about 2 kg/hr. We might expect 0.1 to 0.2 kg/hr of ash to be collected in the baghouse. Thus, in theory, we could get the ash samples from UA. In practice, the baghouse is not emptied or cleaned between runs. We discussed using a high volume sampler to collect the ash samples. Further discussion on the ash samples needs to take place.

- Mike Holmes at McDermott can provide an ash sample of the Ohio blend at nominal stoichiometric ratio; these were obtained at the CEDF.

- Bill Linak from EPA requested some coal (one to two barrels) to generate ash < 2.5 microns for study at EPA. We agreed on samples of the Ohio and Wyodak coals.

- Jerry Huffman, as editor of Fuel Processing Technology, proposed creating a special issue to contain papers from the Phase I program. We went over a list of possible topics and agreed to have first drafts of papers completed by September 1.

- The next review meeting is scheduled for January 14-15, 1999. The location is tentatively going to be Tucson. We will try to coordinate with a DOE and EPRI-sponsored conference on acid rain and air toxics to be held in Tucson from January 11-13, 1999.

A similar program on trace metals in coal and coal combustion is underway in the United Kingdom. The program is being managed by Dr. Rabindra Chakraboty of ETSU. Dr. Chakraboty was contacted and information was sent to him regarding our program. He promised to discuss our program with researchers in the United Kingdom.

3.2 Coal Characterization (UK, USGS, MIT)

3.2.1 *Coal Selection*

We chose four coals for detailed study in Phase I. Variation in source and coal mineralogy were criteria for selection, as well as economic importance. The four coals were as follows: Pittsburgh Seam, Northern Appalachian bituminous coal; Elkorn and Hazard Seams, Eastern Kentucky, low sulfur, "compliance" coal; Illinois 6 Seam, Illinois basin bituminous coal; and Wyodak Seam: Powder River Basin sub-bituminous coal. Pulverized samples were procured and characterized by traditional analyses as well as advanced analyses such as CCSEM, Mössbauer spectroscopy, and XAFS spectroscopy at UK and selective leaching and microprobe at USGS. Analysis of the Phase I coals was documented in the Phase I Final Report and a recently completed Topical Report on Phase I coal selection and characterization.

In the Phase II program, two additional coals were selected for study. We will continue to study one of the Phase I coals. This will make a total of three coals in the Phase II program. The coals were again chosen in an attempt to (1) represent a broad range of elemental forms of occurrence and (2) represent the major coal ranks and commercial coal seams used for pulverized coal power generation in the U.S. The list of Phase II coals includes the Wyodak coal from Phase I and two new coals.

A bituminous coal from Ohio coal was selected for study. The particular coal sample was a blend of three seams: Ohio 5, Ohio 6, and Ohio 7. This blend was made for testing at McDermott Technologies Clean Environment Development Facility (CEDF). The CEDF test program, also sponsored by DOE, is intended to study mercury emissions from coal-fired combustion systems and the interactions of mercury and air pollution control devices such as scrubbers. A similar coal, a blend of Ohio 5 and 6 seams, is burned at a full scale power plant which is currently being sampled for trace element emissions in another DOE-sponsored program. A 1.5 ton sample of this Ohio 5, 6, and 7 blend was obtained directly from the mine. The coal was ground at the CONSOL R&D facility. Thirteen barrels of pulverized coal were shipped to UA. Samples of pulverized coal were then sent to MIT, UK, USGS, and PSI.

The second new coal in Phase II is a lignite from North Dakota (Hagel Bed). This coal is burned at a mine-mouth utility power plant in North Dakota. While lignites are not major steam producing coals throughout the United States, they are important regionally. The mineralogy of lignites from this seam is different from other coals. This coal is also burned at a full scale power plant which will be sampled for trace element emissions in another DOE-sponsored program. A pulverized sample was obtained from EERC. Twelve barrels of pulverized coal were shipped to UA. Samples of pulverized coal were then sent to MIT, UK, USGS, and PSI.

The Wyodak coal will continue to be studied in the Phase II program. This is a sub-bituminous coal from the Powder River Basin and is an important steam coal. More experimental work, particularly large scale combustion studies, remains to be completed for this coal. The Phase I Wyodak sample was obtained through ABB. Since there was not enough of the Phase I material left for Phase II, a fresh sample was procured from a power plant which burns this coal. Both Phase I and Phase II samples came from the same mine, although the samples were mined 2 years apart. Approximately 1.5 tons of coal were shipped from the power plant to EERC. The coal will be pulverized next quarter and shipped to UA.

3.2.2 *Coal Composition*

Samples of the Ohio 5, 6, and 7 coal and the North Dakota lignite were received at USGS and splits of each have been made for analysis. A 250 g split of each coal was sent to Geochemical Testing, Inc. of Somerset, PA for the following determinations: Proximate, BTU, FSI, Ultimate, Ash Fusion, Sulfur Forms. In addition, Air Dry Loss, needed to convert data from an as-determined to an as-received basis, will be measured. Coal samples were sent to Microbeam Technologies (Grand Forks, ND) for ash composition and coal particle size distribution analysis. Table 3-1 summarizes the coal composition analyses. Table 3-2 shows the forms of sulfur analyses. The coal particle size distribution is shown in Table 3-3.

The Ohio coal has a moderate sulfur content (2.6 wt%) which is intermediate between the Phase I Illinois and Pittsburgh coals. The ash is lower in iron than the Illinois and Pittsburgh coals. The North Dakota lignite has a substantial amount of water as well as a moderately high (~10%) ash content. The lignite has more sulfur than the Wyodak coal and about one-third of the sulfur is pyritic, indicating that this coal will have a significant amount of pyrite. This can also be seen from the ash analysis since the ash has a moderate amount of iron oxide. The ash is also high in calcium, magnesium, and sodium. These are probably organically associated to some degree. XRF analysis of the ash was able to detect chlorine (0.1 wt%) in the Ohio coal, but not in the North Dakota lignite. A separate analysis for chlorine with lower detection limits will be carried out on the program coals.

3.2.3 *Coal Mineralogy*

Samples of the Ohio bituminous coal and the North Dakota lignite were received at UK. Head samples of both coals were split out using a riffle-splitter. The remaining sample of the Ohio coal was submitted to B. K. Parekh at the University of Kentucky Center for Applied Energy Research, who will oversee a separation of the sample into float and tailings fractions using one of the flotation methods available to him. These samples, along with samples of fractions of the low-rank coals generated by leaching at USGS, will be used for detailed element speciation and mineral characterization experiments over the next year.

Table 3-1. Coal Properties Phase II Program Coals

	Ohio 5,6, and 7		North Dakota Lignite	
	Dry Basis	As Received	Dry Basis	As Received
Proximate (wt %):				
Fixed Carbon	49.95	48.78	41.46	26.59
Volatile Matter	40.12	39.19	43.90	28.15
Moisture	0.00	2.33	0.00	35.88
Ash	9.93	9.70	14.64	9.38
Ultimate (wt %):				
Carbon	72.77	71.07	60.15	38.57
Hydrogen	4.92	5.07	4.02	6.59
Nitrogen	1.40	1.37	0.65	0.42
Sulfur	2.68	2.62	0.98	0.63
Oxygen	8.30	10.17	19.56	44.41
Moisture	0.00		0.00	
Ash	7.93	9.70	14.64	9.38
Heating Value (BTU/lb):	13,172	12,865	9,969	6,392
Ash Composition (wt% SO_3-free):				
SiO_2	38.1		22.0	
Al_2O_3	39.4		20.4	
Fe_2O_3	13.0		11.8	
TiO_2	2.0		0.5	
CaO	2.2		30.3	
MgO	1.0		8.0	
BaO	0.2		0.5	
Na_2O	0.9		5.1	
K_2O	2.5		1.4	
ClO	0.1		0.0	
P_2O_5	0.5		0.1	

Table 3-2. Forms of Sulfur in Phase II Coals

	Ohio 5,6, and 7		North Dakota Lignite	
	Dry Basis	As Received	Dry Basis	As Received
(in wt%)				
Sulfate Sulfur	0.02	0.02	0.14	0.09
Pyritic Sulfur	1.42	1.39	0.28	0.18
Organic Sulfur	1.24	1.21	0.56	0.36

Table 3-3. Coal Particle Size Distribution for Phase II Coals (in wt%)

Size Range, microns	Ohio 5,6, and 7	North Dakota Lignite
2.2-2.6	0.6	0.3
2.6-3.0	0.8	1
3.0-3.4	1.2	1.2
3.4-4.0	1.4	1.3
4.0-4.6	1.1	0.9
4.6-5.3	1.1	0.9
5.3-6.2	1.2	1.5
6.2-7.2	1.8	2.2
7.2-8.3	3.1	2.9
8.3-9.6	3.3	3.4
9.6-11	2.5	3.1
11-13	2.2	2.9
13-15	3.2	3.1
15-17	5	4.6
17-20	6.4	6.9
20-23	6.6	7.7
23-27	4.7	5.7
27-37	4	4.6
31-36	5.2	5.6
36-42	6.9	7.2
42-49	7.8	7.8
49-57	7.9	7.4
57-66	7.1	6.3
66-76	6.1	5
76-88	4.7	3.7
88-102	3.1	2.3
102-118	1.1	0.8

3.2.4 *Trace Element Volatility*

As part of the Phase I program, researchers from USGS and MIT studied volatility of trace elements by heating under various conditions. Experiments were conducted by USGS to determine the volatility of trace elements by heating the coal samples to 200, 550, and 1000°C in air. Coal samples were placed in an ashing furnace and ramped up to the desired temperature. Concentrations of trace elements were measured before and after heating. No significant loss of trace elements was measured under these conditions.

Experiments were conducted at MIT on the volatility of trace elements during a procedure similar to the ASTM procedure for determination of volatile matter in coal (ASTM D-3175). In this procedure, a coal sample is placed in a platinum crucible. The crucible is lowered into the hot zone of a vertical tube furnace. The furnace temperature for this experiment was 890°C. After holding the crucible in the hot zone for 7 min, it is then removed and weighed to determine the loss of volatile matter. For these tests, the concentrations of trace elements were also determined by NAA after the procedure.

This procedure was carried out for two coal fractions, one from the Elkhorn/Hazard coal and one from the Pittsburgh coal. Both coal fractions were size and density segregated as discussed in the Phase I Final Report. The coal fractions were the high density, large (90 to 106 micron) fractions. Table 3-4 gives the percentage of elements retained in the char after loss of volatile matter. The volatile matter content determined for coals was 36.0% for the Elkhorn/Hazard coal and 36.1% for the Pittsburgh coal; these values are comparable to the volatile matter contents as measured by an analytical laboratory.

Some values are greater than 100 which may be due to errors in measurement. The recovery of Fe is almost 100% which may be expected since the melting point of iron is much higher than the pyrolysis temperature. For some elements, the pyrolysis temperature was higher than the boiling points: K, As, Se, Cd, Cs. These elements were not completely volatilized, although there was substantial loss of Cd, Se, and As, indicating reaction with the ash. On the other hand, significant fractions of Cr, Co, Sc, and La were devolatilized, even though the pyrolysis temperature was less than the melting point of the element. Cr (and probably Co, Sc, and La) are associated with the organic portion of the coal. This experiment provides some preliminary evidence for dependence of the loss of an element during devolatilization on its form of occurrence in the coal. Further investigations will be undertaken in Phase II to determine if this latter procedure can provide any information on the forms of trace elements in coal samples.

3.2.5 *Forms of Occurrence of Trace Elements in Coal*

During the quarter, an experimental session was conducted at beam-line IV-3 at the Stanford Synchrotron Radiation Laboratory (SSRL). Some initial data on arsenic in the Ohio bituminous coal and in some high arsenic coals obtained from colleagues (R. B. Finkelman, H. E. Belkin) at the USGS were also obtained. The latter spectra are shown in Figure 3-1 and indicate a range of arsenic oxidation states from As_2^{2-} to AsO_4^{3-}, in which the formal oxidation states of arsenic are -1 and 5+ respectively. These data will be discussed in more detail in a future report.

Table 3-4. Trace Elements Retained by Char (in wt%) after Devolatilization by ASTM Procedure

Element	Elkhorn/Hazard (KYH90106)	Pittsburgh (PTH90106)
Na	80.5	85.2
K	53.3	63.0
Ca	33.5	142.0
Sc	71.1	88.8
Cr	99.2	28.2
Fe	98.6	100.4
Co	63.3	74.3
Zn	57.9	105.0
As	44.8	73.7
Se	12.8	63.9
Mo	40.0	256.0
Cd	22.4	2.0
Sb	64.0	81.9
Cs	64.0	76.7
La	71.0	93.2
Ce	93.7	135.0

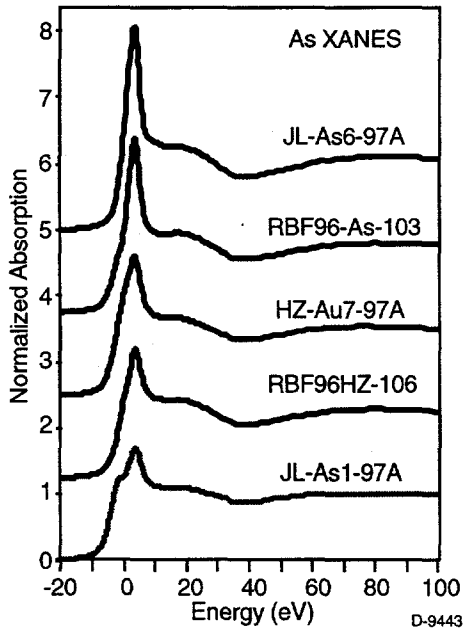

Figure 3-1. Arsenic XANES spectra of USGS high As coals.

3.3 Combustion Zone Transformations (PSI, MIT)

Trace element mass balances were not reported in the Phase I Final Report for the Phase *I* experiments at MIT's Drop Tube Furnace (DTF) and PSI's Entrained Flow Reactor (EFR). Under pyrolysis conditions at the MIT DTF (Table 3-5), good mass balance closure (>80%) was observed for Cr, Fe, Co, As, and Sb. Na and Se did not show good mass balance closure. Table 3-6 gives mass balance closure for selected elements during some of the combustion experiments at MIT. Under combustion conditions, the overall ash mass balance closure was 85%. Therefore, elements with 85% mass balance closure should be acceptable. Iron and arsenic generally show good mass balance closure. Na, Cr, Co, and Sb show somewhat lower values. Care should be taken in use of the vaporization data for Na, Cr, Co, and Sb until better mass balance closures are demonstrated.

Table 3-5. Mass Balance Closure in MIT DTF under Pyrolysis Conditions (in wt%)

Sample	Na	Sc	Cr	Fe	Co	As	Se	Sb
PTH90106	55	60	103	93	91	104	34	108
WYH90106	47	79	56	128	67	105	44	109

Table 3-6. Mass Balance Closure in MIT DTF under Combustion Conditions (in wt%)

Sample	$\%O_2$	Na	Cr	Fe	Co	As	Sb
KYH90106	20%	83		87	60	83	63
PTH90106	10%	63	33	233	115	137	361
PTH90106	20%	63	68	94	33	106	55
PTH90106	35%	63	61	62	51	58	52
PTH90106	50%	78	48	99	60	83	54

Mass balances were compiled for the PSI experiments (Table 3-7). Poor (high) mass balance closure was observed for Cr and Cd which can be attributed to contamination. A project involving cadmium sorbents was conducted in the furnace before the Phase I program and there may have been some residual Cd outgassing from somewhere. The high Cr numbers may be due to contamination from stainless steel. Low mass balance closure was generally seen for Br, As, Se and Sb. Other elements had acceptable mass balance closures.

Table 3-7. Mass Balance Closure for PSI EFR Experiments

Run	22	10	27	33	52	40	3	2			
Coal	EH	I6	I6	I6	P8	P8	EH	WY			
SR	1.2	1.2	0.9	1.2	1.2	1	1.2	1.2			
Ash Mass Closure	125%	24%	179%	272%	15%			22%	106%		
Element									Average	Minimum	Maximum
Na	67%	122%			63%	90%	129%		94%	63%	129%
Ca			762%					5423%			
Sc	79%	139%	72%	146%	75%	92%	142%	122%	108%	72%	146%
Cr	134%	703%	159%	169%	196%	-24%	188%	93%	202%	-24%	703%
Fe	102%	98%	83%	146%	39%	196%	184%	28%	110%	28%	196%
Co	83%	122%	68%	126%	83%	128%	128%	58%	100%	58%	128%
Zn	21%	44%	31%	67%	55%	199%	218%	20%	82%	20%	218%
As	29%	40%	24%	75%	30%	67%	72%	41%	47%	24%	75%
Se	20%	51%	21%	27%	27%	190%	49%	31%	52%	20%	190%
Br	34%	192%			26%	6%	15%		55%	6%	192%
Rb	119%	99%			64%	131%	285%		140%	64%	285%
Mo	72%	150%			164%	174%	122%		136%	72%	174%
Cd	93%	2263%			181%	660%	109%		661%	93%	2263%
Sb	32%	59%	*6533%*	85%	45%	72%	85%	68%	64%	32%	85%
Cs	87%	107%			78%	96%	217%		117%	78%	217%
Ba	74%	138%			78%	82%	79%		90%	74%	138%
La	82%	119%			83%	96%	139%		104%	82%	139%
Ce	71%	127%			75%	95%	136%		101%	71%	136%
Sm	82%	129%			80%	91%	142%		105%	80%	142%
Eu	92%	123%			66%	110%	167%		112%	66%	167%
Yb	83%	2106%			76%	96%	139%		500%	76%	2106%
Lu	85%	2225%			85%	105%	145%		529%	85%	2225%
Hf						382%	153%				
Au		170%									
Hg		14%			19%	474%	69%				
Th	84%	2441%				98%	143%				
U						95%	142%				

3.4 Post-Combustion Transformations (UA, UK, PSI)

3.4.1 *Large Scale Combustion Studies*

Radionuclide Post-combustion Transformation Mechanisms

Additional statistical analysis of Phase I data was performed to investigate mechanistic information related to the fate of the radionuclides Cesium, Thorium, and Cobalt during the combustion of Pittsburgh seam coal and Illinois #6 coal. The results are summarized in Figures 3-2 through 3-16. A description of the methods used to generate these data is presented in the Phase I final report.

Nucleation can be explored by examining the effect of resident time/temperature on the distribution and composition of submicron particles. Homogeneous nucleation will result in a correlation between the change in trace metal concentration in submicron particles and the change in the overall distribution of submicron particles. Figures 3-2 through 3-4 show mass fraction distributions for Cs, Th, and Co, respectively. If this mechanism is important, Figures 3-2 through 3-4 should show an increase in specie mass fraction for the submicron particles for samples collected from Port 12 compared to Port 4B similar to the increase in total mass fraction shown in the overall particle size distribution (see Figure 3-131, p. 3-176 of the Phase I final report for the overall particle size distribution). These figures suggest that nucleation may be occurring for cesium and thorium in the post-combustion phase for the Pittsburgh coal. There was no evidence of nucleation for cesium and thorium from combustion of the Illinois coal or for cobalt from combustion of either coal.

Log-log plots were constructed of concentration versus particle size for Cs, Th, and Co collected in the Port 12 samples to provide insight into heterogeneous partitioning mechanisms. When a negative slope of –1 occurs, the profile follows a $1/d_p$ (particle diameter) dependence which indicates that surface (heterogeneous diffusion-limiting) reaction may be the dominant formation mechanism. A negative slope of –2 indicates that the profile follows a $1/d_p^2$ dependence and that gas film transfer (condensation) is most likely the dominant formation mechanism. The results are shown in Figures 3-5 through 3-7 for the Illinois fly ash and Figures 3-8 through 3-10 for the Pittsburgh fly ash. From these figures, heterogeneous reaction appears to be the dominant transformation mechanism for all three elements when burning either coal.

In Figures 3-11 through 3-13, the concentration of Cs, Th, or Co on a given plate is plotted versus the corresponding Ca concentration for the Illinois test runs, respectively. Figures 3-14 through 3-16 show the same information for the Pittsburgh test runs. These plots investigate whether Ca-radionuclide complexes are important to radionuclide deposition. It was found that there is a correlation between ash particle Ca concentration and the concentration of Cs and Th when burning Pittsburgh coal. This suggests that Ca complexes may be important for these elements. No correlation was observed for Ca with Cs or Th when burning Illinois coal or for cobalt from the combustion of either coal.

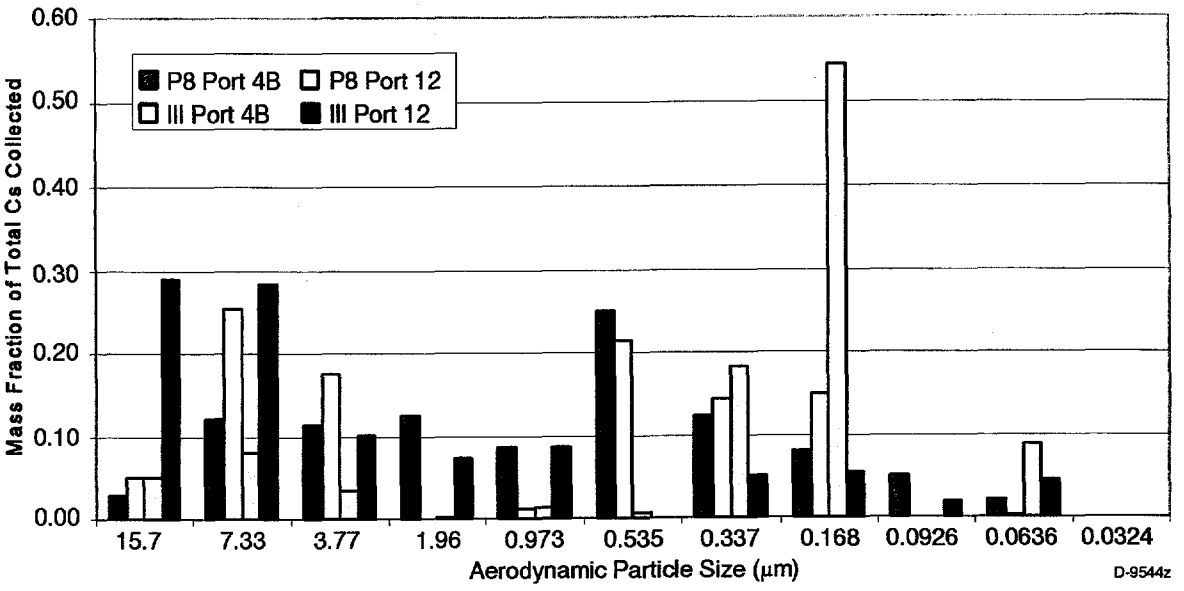

Figure 3-2. Typical Cesium distributions for Illinois #6 and Pittsburgh coals.

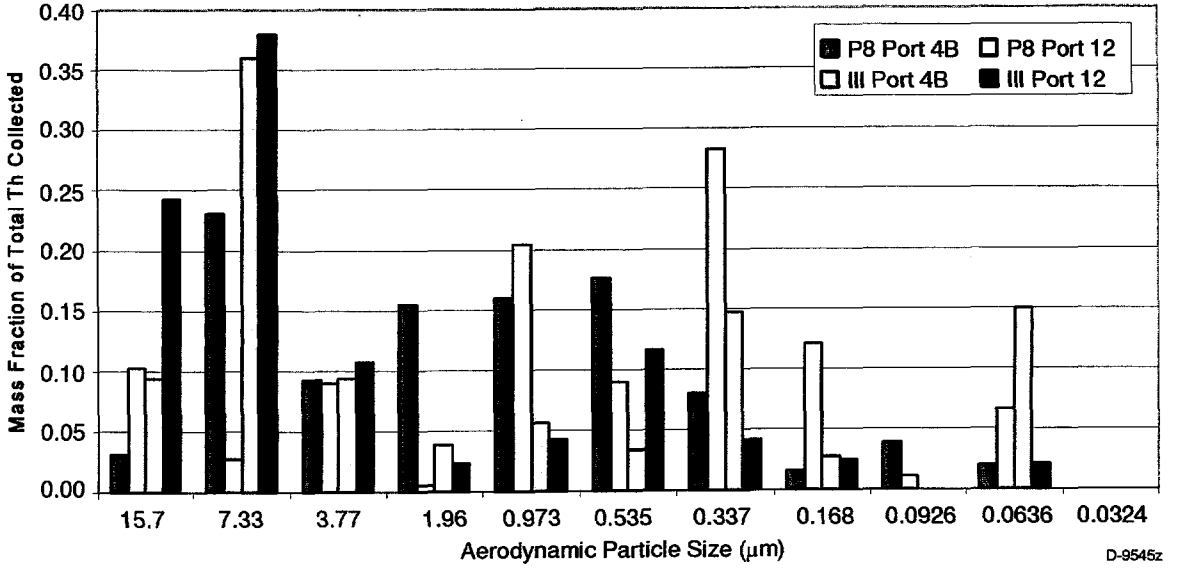

Figure 3-3. Typical Thorium distributions for Illinois #6 and Pittsburgh coals.

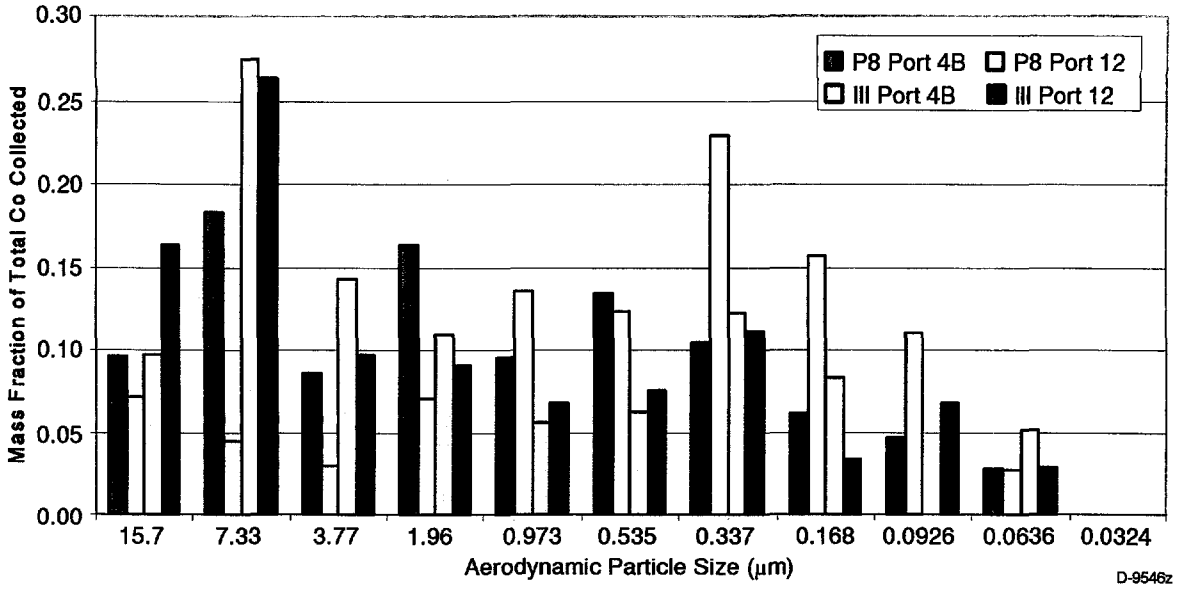

Figure 3-4. Typical Cobalt distributions for Illinois #6 and Pittsburgh coals.

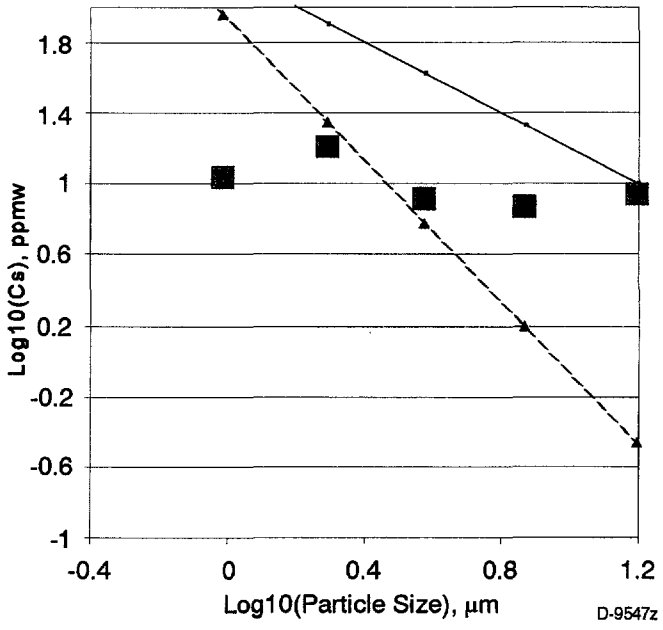

Figure 3-5. Particle size dependence of Cs generated by combustion of Illinois #6 coal.

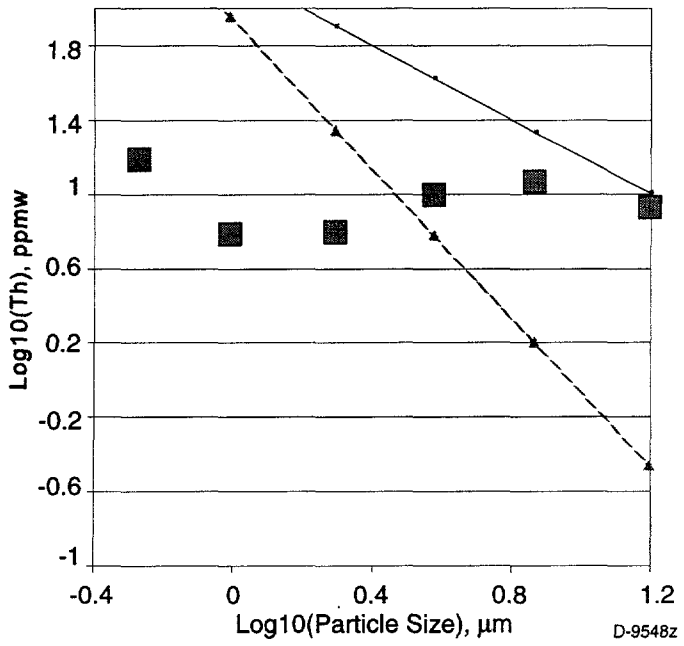

Figure 3-6. Particle size dependence of Th generated by combustion of Illinois #6 coal.

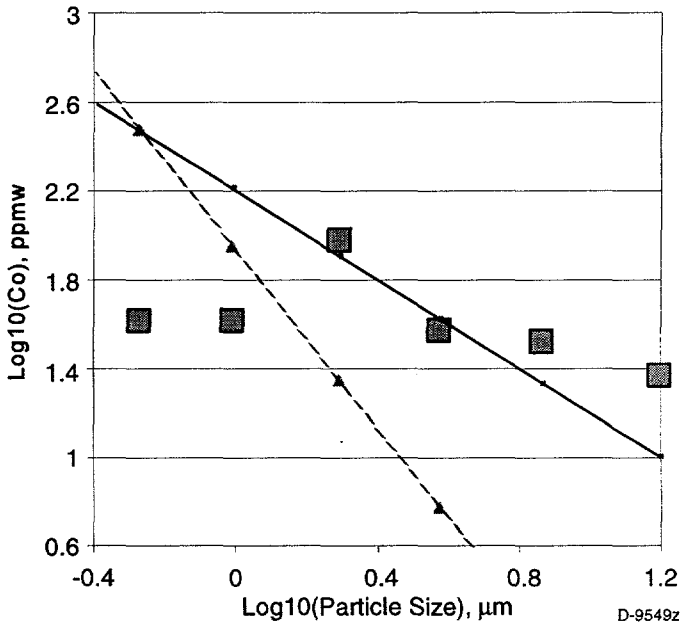

Figure 3-7. Particle size dependence of Co generated by combustion of Illinois #6 coal.

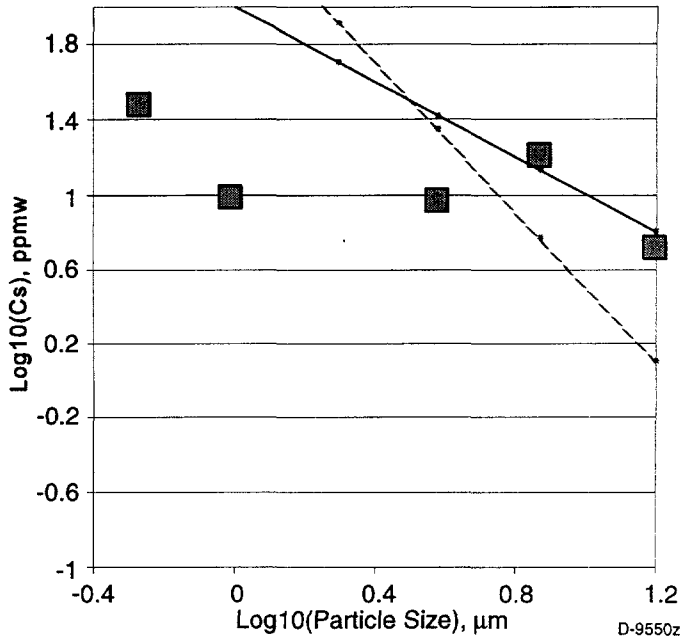

Figure 3-8. Particle size dependence of Cs generated by combustion of Pittsburgh Seam coal.

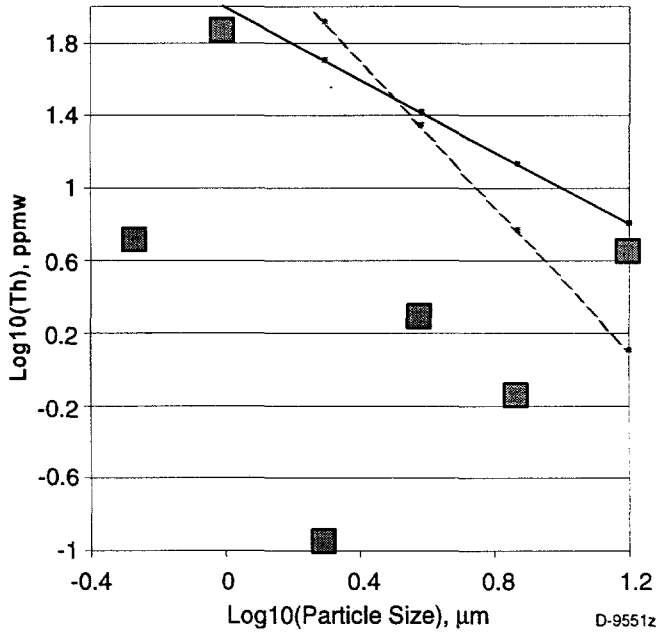

Figure 3-9. Particle size dependence of Th generated by combustion of Pittsburgh Seam coal.

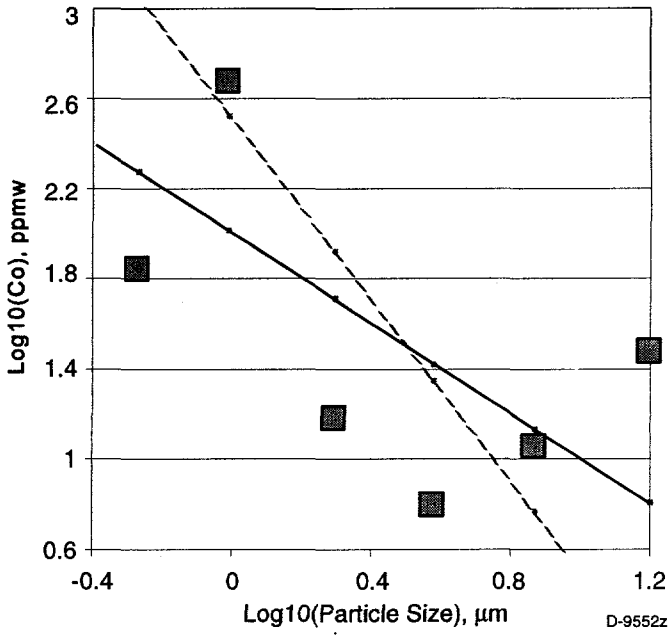

Figure 3-10. Particle size dependence of Co generated by combustion of Pittsburgh Seam coal.

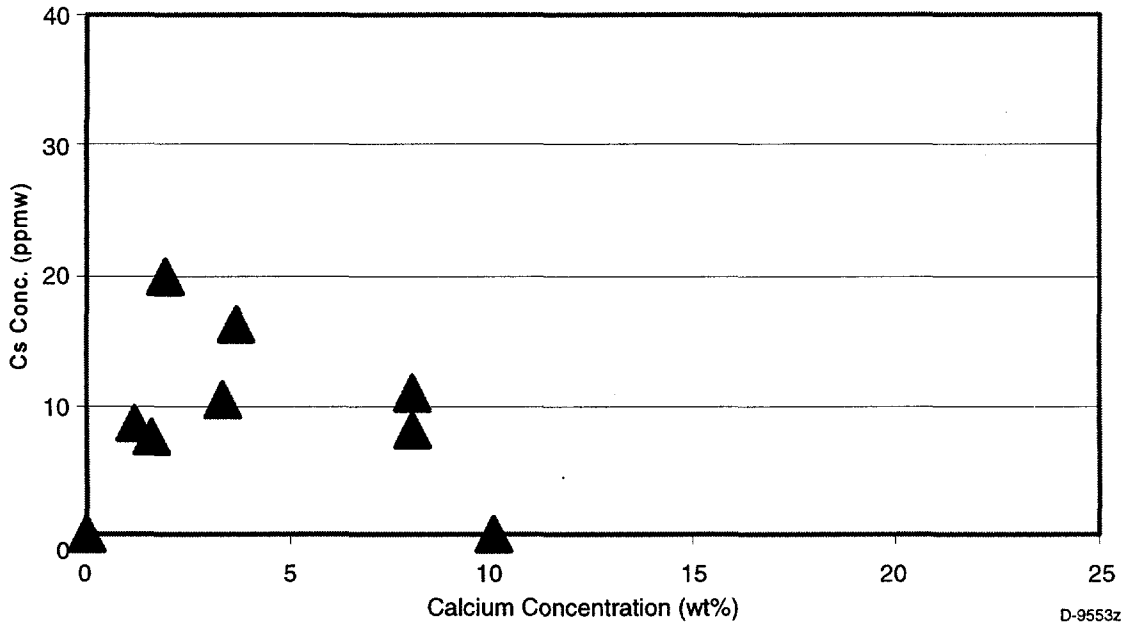

Figure 3-11. Cesium-Calcium correlation for Illinois #6 coal.

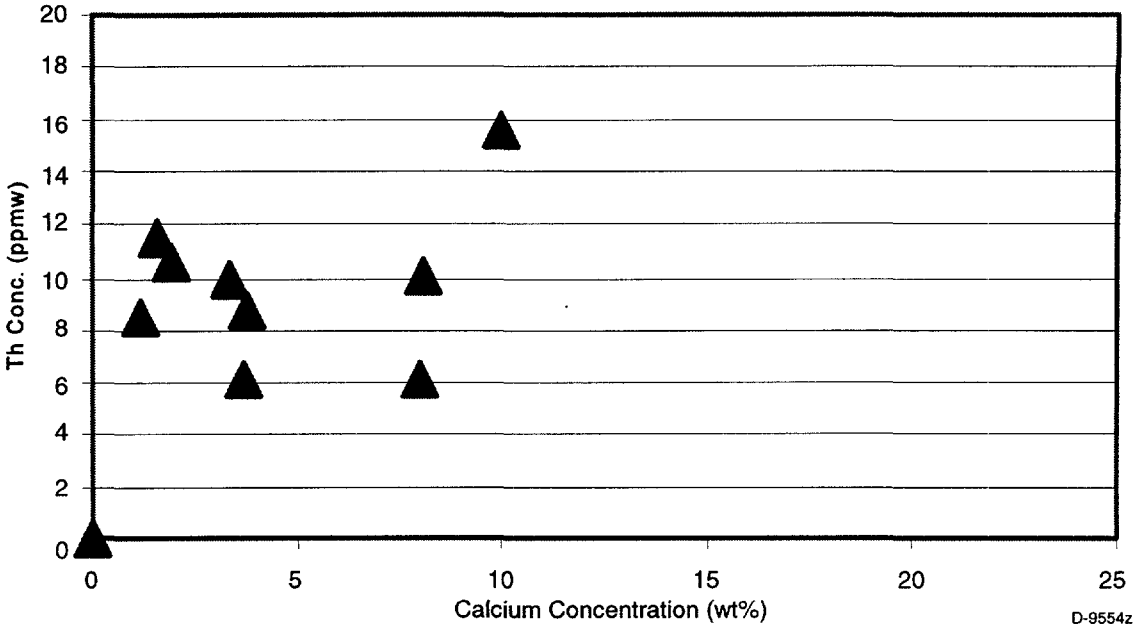

Figure 3-12. Thorium-Calcium correlation for Illinois #6 coal.

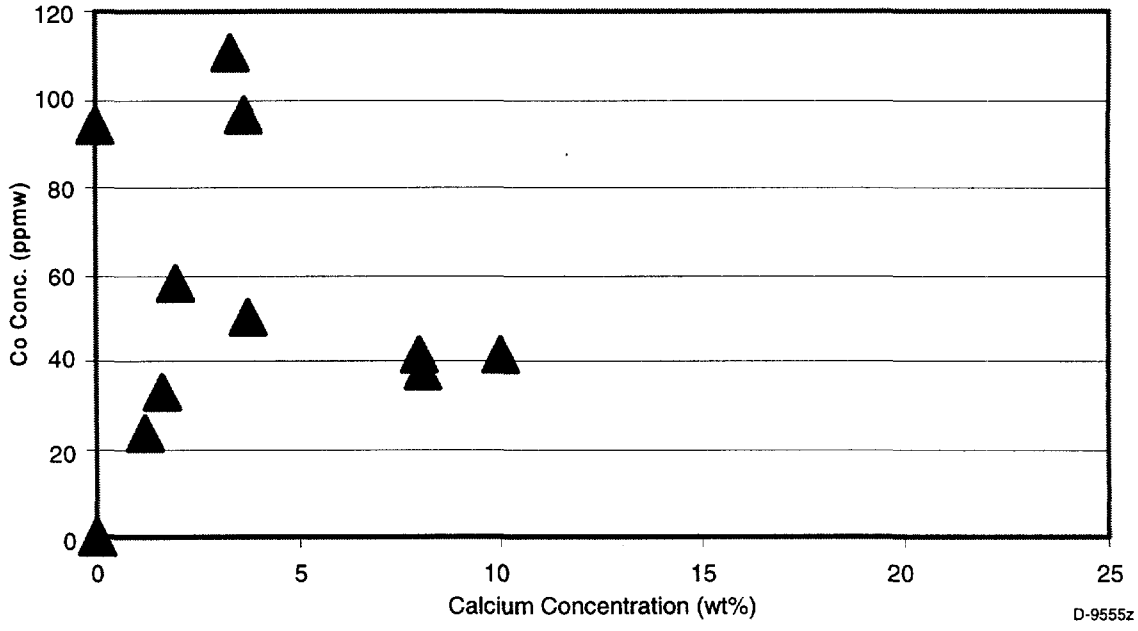

Figure 3-13. Cobalt-Calcium correlation for Illinois #6 coal.

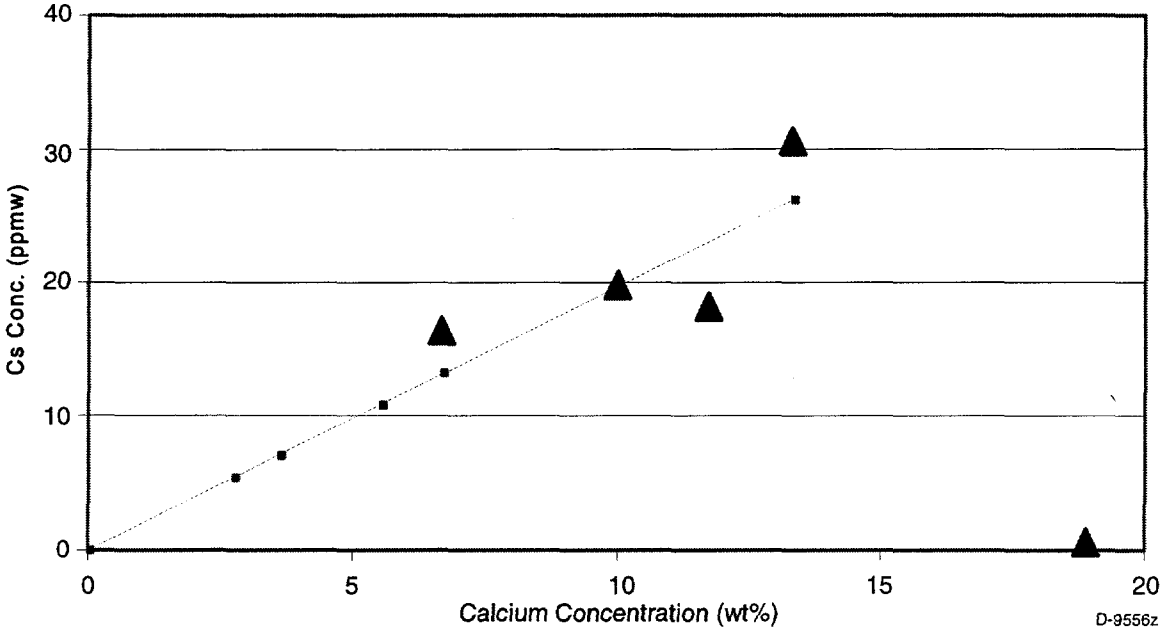

Figure 3-14. Cesium-Calcium correlation for Pittsburgh Seam coal.

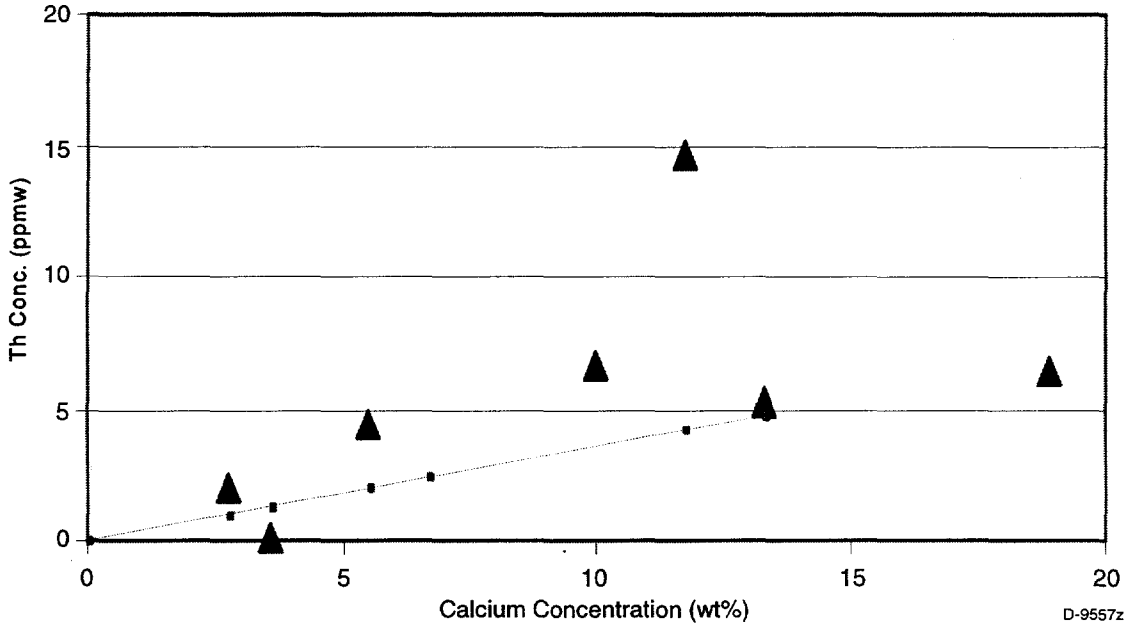

Figure 3-15. Thorium-Calcium correlation for Pittsburgh Seam coal.

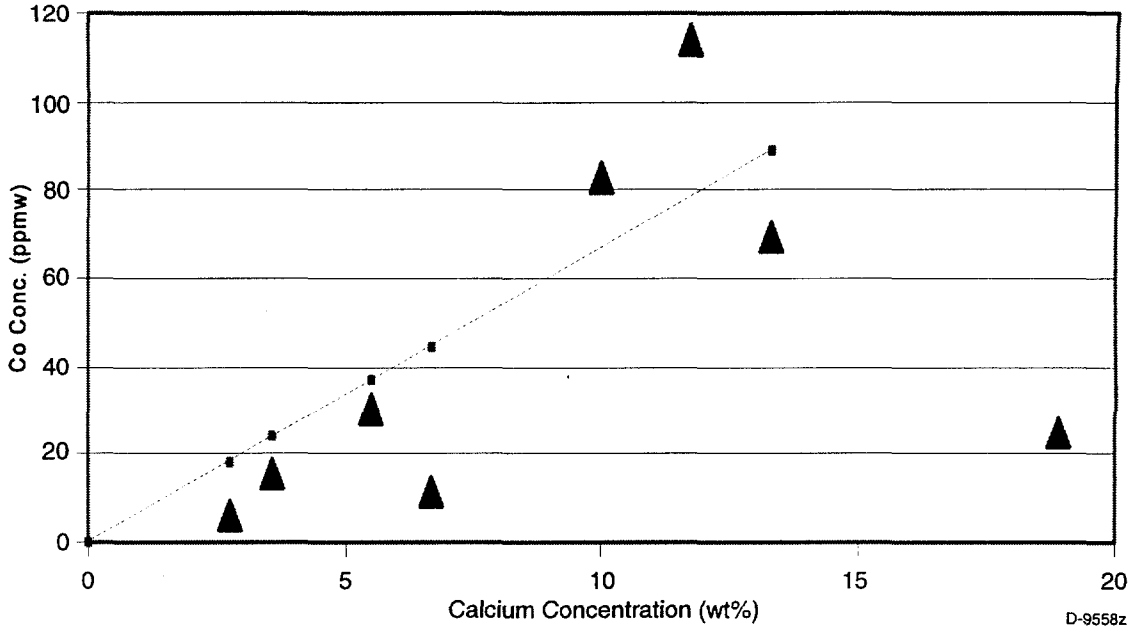

Figure 3-16. Cobalt-Calcium correlation for Pittsburgh Seam coal.

Additional Phase I Arsenic Data

Analytical methods were developed to analyze trace metals using graphite furnace atomic spectroscopy (GFAA). These methods were applied to additional Phase I impactor data to determine the concentration of Arsenic in Pittsburgh fly ash samples.

A comparison of the results from this analytical effort to those previously obtained at MIT using neutron activation analysis (NAA) are shown in Figures 3-17 and 3-18. Also shown on the same figures is a comparison of the total mass of sample collected. The accuracy of the mass of ash collected can greatly influence the reported concentrations. The results shown in Figure 3-17 are for samples collected from Port 4B, located just at the end of the combustion zone. There is fairly good agreement between the results from the two methods. Results in Figure 3-18, collected from Port 12, do not show as good an agreement for the larger particle sizes. The mass of samples collected on these plates is very similar and this does not explain the discrepancy.

Further work on As and other elements will continue during the next quarter to supplement the original NAA-generated results.

3.4.2 *Identification of Mercury Species in Sorbents*

During the quarter, an experimental session was conducted at beam-line IV-3 at the Stanford Synchrotron Radiation Laboratory (SSRL). New mercury sorbent samples from both UA and PSI were the main suites of samples investigated under the auspices of the current program. The PSI sorbent samples are zeolites which were exposed to mercury in coal

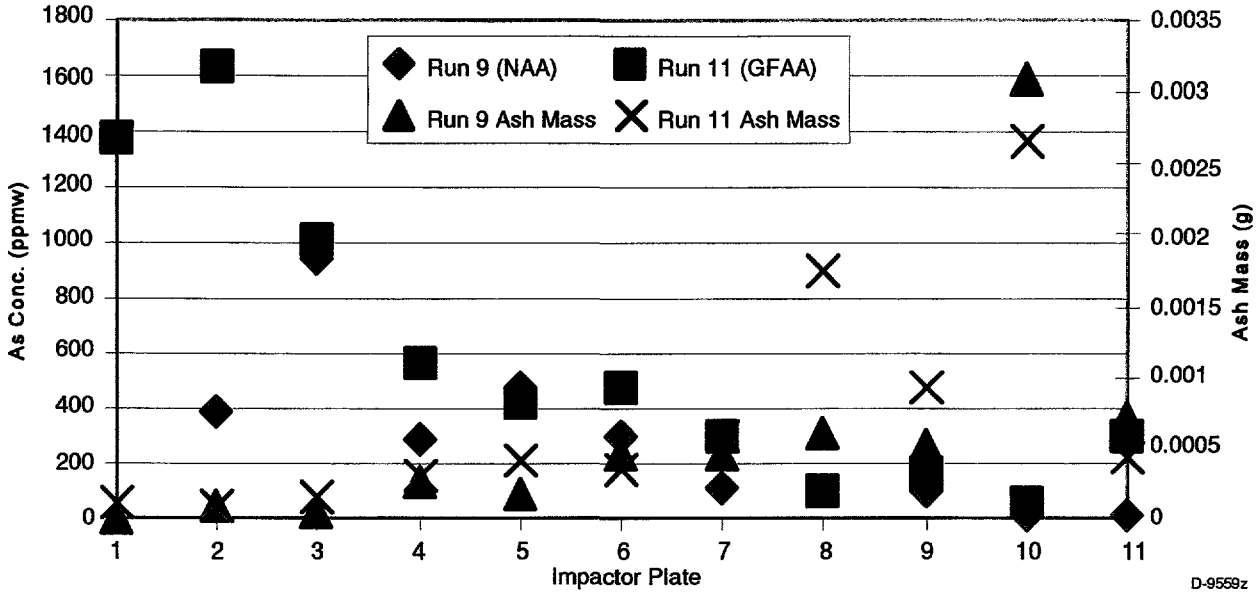

Figure 3-17. Comparison of NAA and GFAA As results for Pittsburgh ash sampled at the end of the combustion zone (Port 4B).

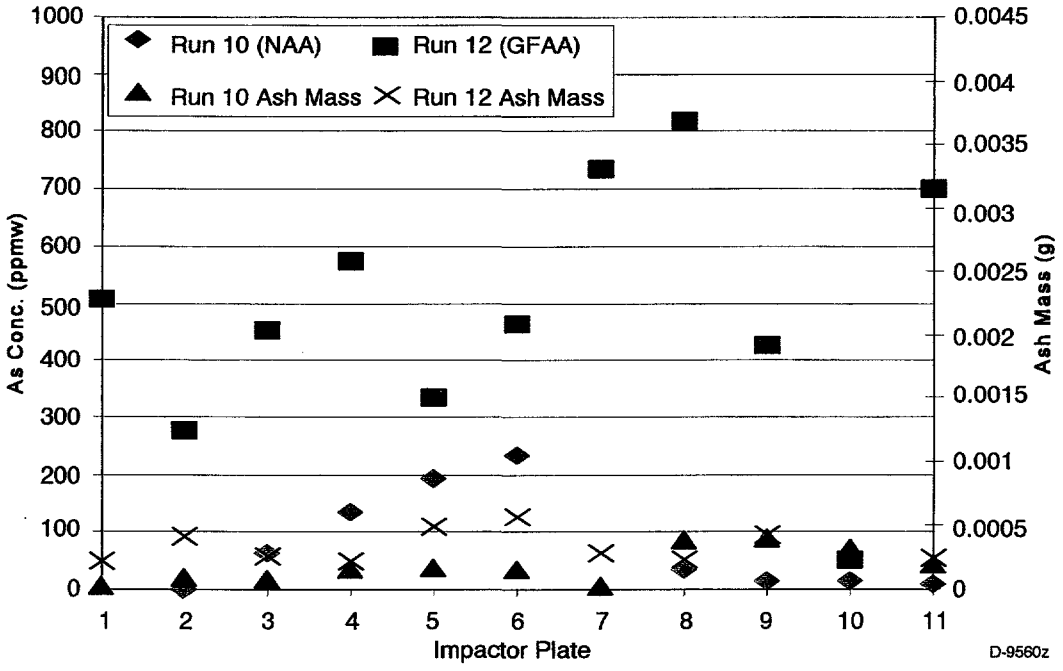

Figure 3-18. Comparison of NAA and GFAA As results for Pittsburgh ash sampled in the post combustion zone (Port 12).

combustion flue gas on another DOE-sponsored program. Some ten samples from UA and six samples from PSI were received and run at the mercury L_{III} edge at 12,284 eV. The samples investigated varied from a mercury content of 8.5 wt% to 8 ppm and the spectra were all obtained in fluorescence geometry using a Lytle detector for the concentrated samples and a 13-element germanium detector for less concentrated samples. In both cases, Soller slits and gallium filters were used to enhance the signal/noise ratio. Counting times varied from a single scan taking about 45 min to multiple scans lasting as much as 8 hours. Experimental and data analysis procedures were the same as described in the Final Report for Phase I of the project.

The mercury XANES data for the UA samples are shown in Figures 3-19 and 3-20 and for the PSI samples in Figure 3-21. The spectra look quite similar; however, as discussed in detail below, there are some quite subtle differences among the different samples that appear to correlate with differences in the samples preparation, chemistry, or conditions of sorption. In addition, the EXAFS data for the UA was sufficiently strong to provide good radial structure functions (RSFs). These are shown in Figures 3-22 and 3-23. Again, they are very similar and all indicate a Hg-nearest neighbor (NN) phase-shift uncorrected distance of about 2.0 ± 0.1. The PSI samples were too low in Hg to provide sufficient EXAFS signal for a useful RSF.

During the course of this project (Phase I through the present), we have accumulated much XAFS data on mercury in various sorbents and on a wide range of Hg compounds. Almost without exception, the first features that occur on the mercury absorption edge are two inflection points (Figure 3-24), whose positions and intensities appear to be related to chemical bonding differences. In particular, the separation of these inflection points appears to correlate with differences in the ionicity of the Hg-NN bond. The more ionic compounds of mercury, such as HgO, mercury sulfate, etc., in which the Hg ion is surrounded by oxygen anions, have large

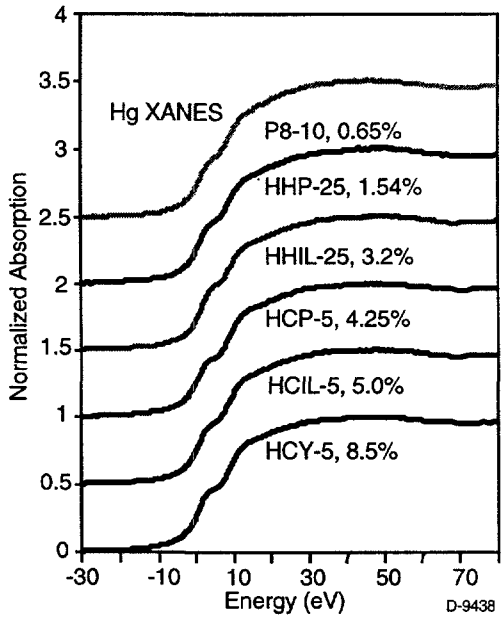

Figure 3-19. Hg XANES spectra of high mercury sorbent samples prepared at UA.

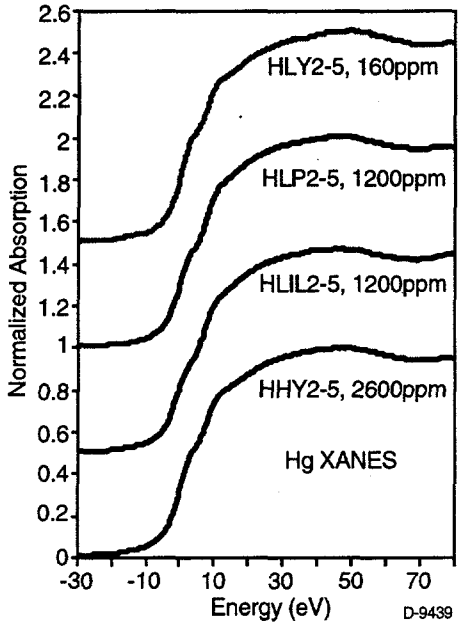

Figure 3-20. Hg XANES spectra of low mercury sorbent samples prepared at UA.

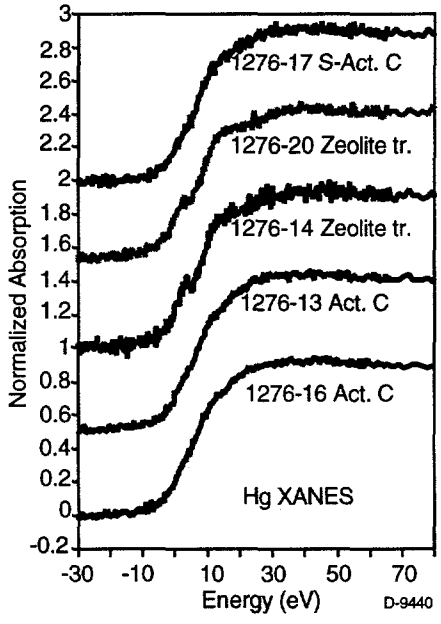

Figure 3-21. Hg XANES spectra of very low mercury sorbent samples prepared at PSI.

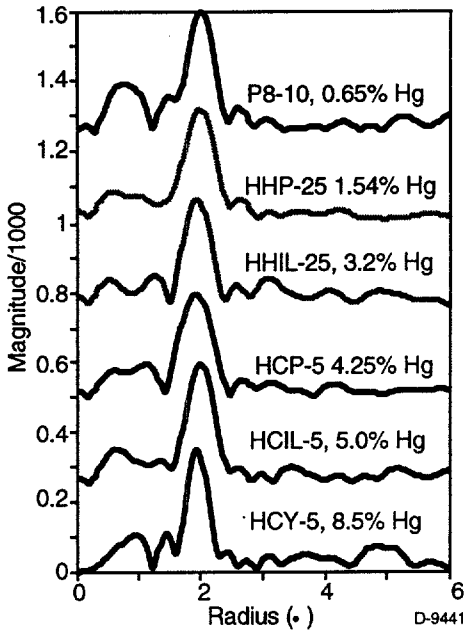

Figure 3-22. Hg RSFs for high mercury sorbents prepared at UA.

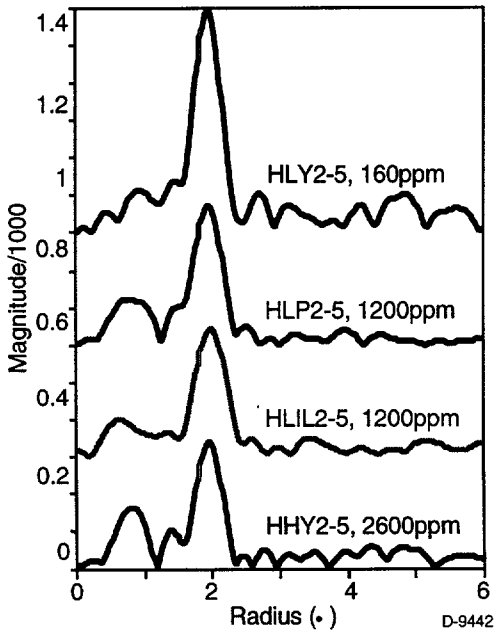

Figure 3-23. Hg RSFs for low mercury sorbents prepared at UA.

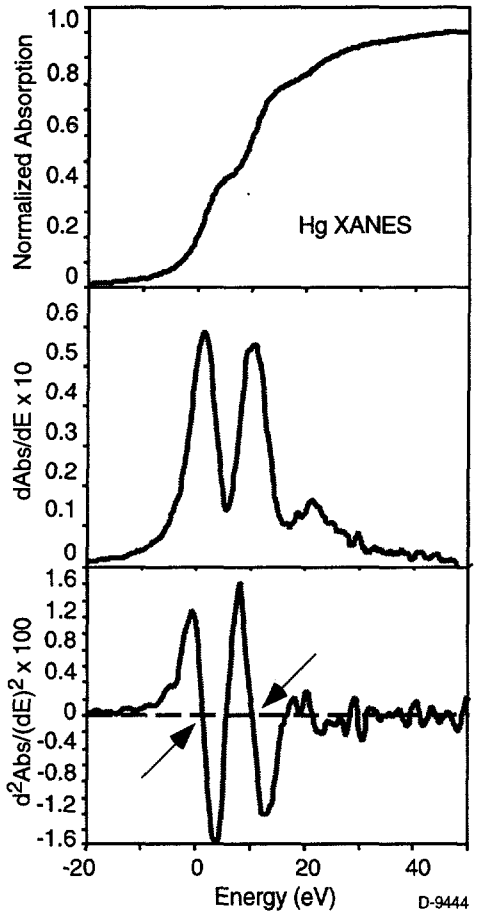

Figure 3-24. Determination of inflection point difference (IPD) from Hg XANES spectra. Arrows indicate measurement points.

values for the separation of the inflection points, whereas the least ionic species such as Hg iodides and diphenyl mercury have small separations. The data for this inflection point difference (IPD) are presented in the Table 3-8 for 13 mercury compounds. Interestingly, it seems to make little difference whether the mercury is Hg(I) or Hg(II) as the two sulfates and the two chlorides have essentially the same IPD values.

The procedure used to obtain the IPD data shown in Table 3-8 is based on the double differentiation of the smoothed XANES spectrum (Figure 3-24) to obtain the $d^2X/(dE)^2$ spectrum and the positions of the inflection points are then indicated by where this function crosses y=0 most steeply. This new procedure was done for all the Hg XANES spectra that we have taken over the last 18 months and is tabulated in Table 3-9 for various suites of samples. Values obtained from activated carbon samples obtained from the Illinois State Geologic Survey (ISGS) are included in this table.

Table 3-8. Hg XAFS Systematics for Mercury Compounds

Hg Compound	*IPD eV*	*RSF, A*
HgO (calc.)	13.3	
HgO (ref)	13.3	1.72
Hg Acetate	10.6	1.68
Hg2SO4	9.6	
HgSO4	9.5	
Hg2Cl2	8.4	
HgCl2	8.4	2.02
HgS (red)	7.5	2.05
HgCH3I	6.9	2.49
Hg diphenyl	6.8	
HgI2	6.5	
HgKI4	4.6	2.52

Table 3-9. Mercury XANES Systematics for Sorbent Samples

Source of Sorbent/XAFS	*Sorbent*	*Coal/Hg Vapor*		*IPD, eV*
U. Arizona Samples/SSRL	HIL-25	IL	Hg	8.4
	HIP-35	Pt	Hg	8.1
	HIL-25	IL	Hg	8.0
	HIY-25	Wy	Hg	7.9
	HY-25	Wy	Hg	7.6
	LY-25	Wy	Hg	7.6
U. Arizona Samples/SSRL	HCP-5	Pt	HgCl2	8.4
	HCY-5	Wy	HgCl2	8.3
	CIL-5	IL	HgCl2	8.1
	PS-10	Pt	Hg	8.0
	HIL-25	IL	Hg	8.0
	HLP-35	Pt	Hg	8.0
	HHL-25	IL	Hg	7.9
	HHP-35	Pt	Hg	7.8
	HHY-25	Wy	Hg	7.7
	HLY-25	Wy	Hg	7.3
ISGS/Radian	ISGS-2	Char	HgCl2 +	9.1
	ISGS-4	Char		9.0
	ISGS-1	Char	Hg + NOx	8.9
	ISGS-5	FGD		8.5
	ISGS-3	Char	Hg	8.2
PSI Sorbent Samples/SSRL	PSI-20	Zn, treat		10.0
	PSI-14	Zn, treat		9.0
	PSI-13	AC, treat		6.9
	PSI-17	AC, treat		6.9
	PSI-16	AC		6.1

A histogram of the distribution of the values is displayed in Figure 3-25 and it clearly indicates separate regimes for the different suites of samples, although there is some degree of overlap. When we compare the IPD values for the sorbents with those for the standards, we find that most of the UA and ISGS samples have values comparable to chlorides and sulfides. However, the values for the PSI carbon samples are significantly lower, whereas the values for the PSI zeolite samples are significantly higher than all of the UA and most of the ISGS samples. Moreover, it appears that within the different groups the sorption experiments done with $HgCl_2$ give rise to higher IPD values than the experiments done with mercury vapor (Hg^0). Finally, within the UA samples, it appears that the Wyodak samples have smaller IPD values than either the Pittsburgh or the Illinois samples when exposed to Hg^0 vapor.

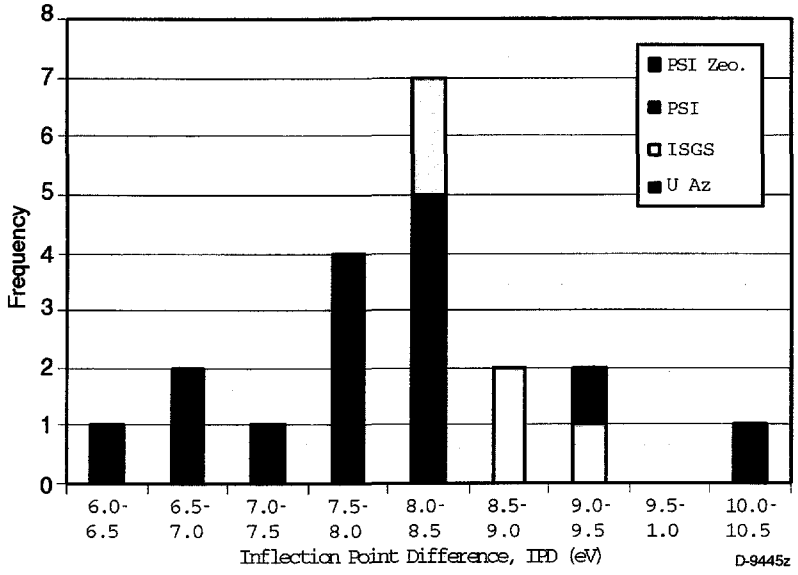

Figure 3-25. Distribution of IPD values for mercury sorbents.

Although there appear to be some quite definite systematics in these IPD data, without knowing more details of some of the samples, their preparation and Hg sorption experiments, it is premature perhaps to speculate the significance of these trends. However, it is interesting to note that many of the UA IPD values are compatible with chloride and/or sulfide as the coordinating ligand around mercury. Figure 3-25 makes an interesting point too, in that it does not show a two-peaked distribution around the values for HgS and $HgCl_2$. This may perhaps suggest that Hg coordination reflects the S/Cl ratio at the sorption sites rather than the formation of a specific sulfide or chloride species, i.e., an "average" $HgS_xCl_{2(1-x)}$ species rather than HgS or $HgCl_2$. In this regard it is worth noting that the chlorine content of the Wyodak coal is much less than those of the two bituminous coals; hence, its IPD values reflect principally sulfide bonding under Hg^0 vapor.

For the PSI sorbent samples, the values are outside the chloride/sulfide range. The zeolite samples are higher, whereas the activated carbon samples are lower. For the zeolite samples, it is reasonable to speculate that the mercury is bonded to the oxygen anions in the aluminosilicate framework structure of the zeolite. Certainly the IPD values for the zeolite sorbents are compatible with oxidic species, such as the sulfate species. The activated carbon samples, however, may indicate that the principal bonding is between Hg and C, as the IPD values are closest to that of diphenyl mercury. It was also noticed in the XAFS spectra of the PSI sorbents that a small absorption edge for selenium was usually also present. Possibly a Hg-Se species might also contribute to the low IPD values, as mercury selenides are less ionic than mercury sulfides.

3.4.3 *Mercury-Char Interactions*

In the Phase I program, researchers at UA carried out the first detailed characterization of unburned carbon as a sorbent for mercury. Vapor phase mercury was produced from both elemental and mercury chloride sources. Chars generated from three coals (Pittsburgh, Illinois 6 and Wyodak) were used as sorbent material. The temperature of the source as well as the char sorbent was carefully controlled.

In the reporting period, new analysis of the forms of sulfur using sulfur XANES data and analysis was performed on the Wyodak char sample. The XANES data were collected during a short trip to the National Synchrotron Light Source (NSLS) in June. Addition of the forms of sulfur data completes the data analysis of these data. The results from the Phase I Final Report have been recalculated and will be presented here.

The coals studied have a variety of forms of sulfur as shown in Table 3-10. The data indicate that the Pittsburgh and Illinois No. 6 coals contain significant amounts of both pyritic and organic sulfur. The Wyodak coal contains primarily organic sulfur.

Table 3-10. Forms of Sulfur in Coals

	Pittsburgh		Illinois No. 6		Wyodak	
Sulfur (wt%, dry basis)	2.12		3.82		0.46	
Forms of sulfur:	Wt % in Coal (Dry Basis)	Percent of Total Sulfur	Wt % in Coal (Dry Basis)	Percent of Total Sulfur	Wt % in Coal (Dry Basis)	Percent of Total Sulfur
Sulfate	0.01	0.5	0.04	1.0	0.02	4.3
Pyritic	0.91	42.9	1.57	41.1	0.03	6.5
Organic	1.2	56.6	2.21	57.9	0.41	89.1

The chars were made by reacting the coals in the PSI Entrained Flow Reactor (EFR), a three-zone electrically heated furnace. Coal is burned in a laminar flow furnace with a diameter of 8.57 cm. The gas temperature in the furnace can be varied from 1200 to 1750 K with an oxygen partial pressure between 0 and 1. Coal particles are fed into the top of the furnace and char particles drawn into a nitrogen-quenched probe and collected on a filter. Two coal chars

(Pittsburgh and Illinois 6) were made using a stoichiometric ratio of 0.6 and gas temperature of approximately 1723 K. The Wyodak char was made by devolatilizing the coal in the EFR in nitrogen at approximately 1723 K. The ash content of the chars and surface area of the chars was measured at PSI and the sulfur content was determined by Galbraith Laboratories (Knoxville, TN), as summarized in Table 3-11.

Table 3-11. Properties of Chars for Mercury Sorption Experiments

	Pittsburgh	Illinois 6	Wyodak
Carbon Content, wt% LOI	69%	39%	83%
BET surface area, m^2/g	126	94	147
Total Sulfur, wt%	2.07%	4.09%	0.96%

In this work, XAFS spectroscopy is used to understands the speciation of minor and trace elements. The forms of sulfur in the chars were determined using XAFS spectroscopy. Sulfur XANES spectra were analyzed according to least-squares fitting procedure developed for sulfur in coals and chars.[1] Estimates of the %S in different forms in the chars are given in Table 3-12.

Table 3-12. Forms of Sulfur in Chars by XAFS Analysis

	Pittsburgh	Illinois 6	Wyodak
Sulfate	5%	2%	20%
Pyrrhotite	20%	35%	----
Elemental Sulfur	25%	35%	17%
Organic Sulfide	50%	29%	63%

Sorption experiments were performed at UA at two temperatures, 343 and 433 K. Details of the experimental apparatus can be found in the Phase I Final Report. All the experiments were done under oxidizing conditions where the gas composition was: N_2 80%, CO_2 15%, O_2 3% and H_2O 2%; a so-called simulated flue gas (SFG). The total flow rate was controlled at 200 scc/min. In order to deliver this SFG composition, air, nitrogen and carbon dioxide gases were used along with a water saturator. The flow of each gas was controlled by flow controllers. The concentration of mercury in the gas phase was calibrated by measuring the weight change of the mercury source. The weight of the mercury source before and after calibration was measured by an analytical balance with up to four-digit accuracy. Gas flow rates were measured and controlled by flow controllers. The gas concentration was then calculated by using the weight difference and the gas flow rate. A typical calibration procedure started by heating up the experimental system to the desired temperature, turning on the SFG and then placing the mercury source into

the source reactor. No sorbent was placed into the sorbent reactor at this time. The duration of the calibration was usually between 50 and 150 hours.

The calibration of mercury chloride concentration was done in a similar procedure, but may not be as accurate due to several factors. First, the water content in the mercury chloride source was unknown. Second, a color change of the source from white to gray was observed before and after the calibration, which indicates a possible reaction of mercury chloride with water or decomposition of mercury chloride. As a result, the calibration accuracy based on the weight change could be affected. The concentration of mercury in the reactant was determined by cold vapor atomic absorption, done by Galbraith Lab. The data were used to determine the sorption ability and capacity of sorbent.

Figure 3-26 gives the results of mercury adsorption at 343 K with a vapor-phase concentration of elemental mercury of 0.35 ppmw and 3.3 ppmw. The horizontal axis represents the duration of the experiment in hours. The vertical axis indicates the mercury content of the chars after the duration of the experiment. For the lower concentration of about 0.35 ppmw , the rate of adsorption appears slower and the adsorption is more than twice as high at higher concentration then at the lower one. However, the higher concentration of 3.3 ppmw is about 10 times higher then the lower concentration of 0.35 ppm, which indicates that the concentration effect to the adsorption of mercury may not be linear, and therefore the adsorption may not be first order in the concentration range tested.

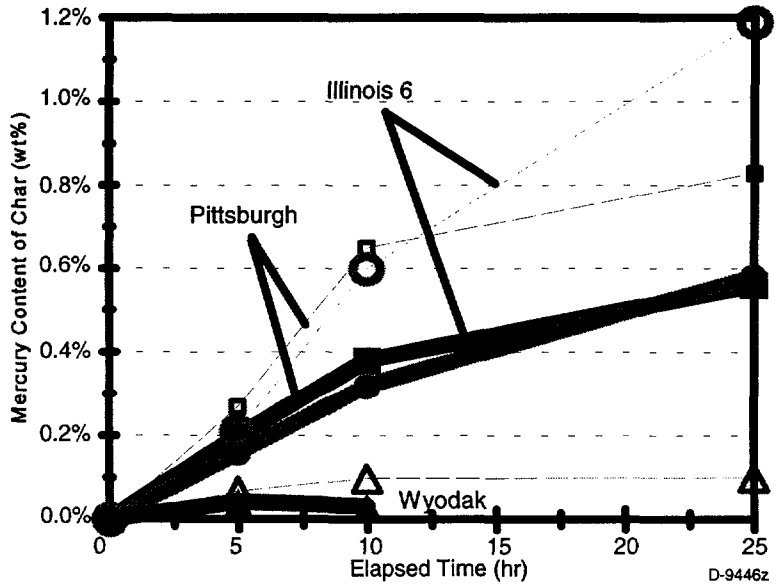

Figure 3-26. Comparison of sorption of elemental mercury at 343 K at two different concentrations: 0.35 ppmw (closed symbols) and 3.3 ppmw (open symbols).

Comparing these three chars, it appears that Illinois 6 and Pittsburgh chars have about the same initial adsorption rate for elemental mercury at 343 K and the Illinois 6 char has higher mercury absorption capacity. Wyodak has the lowest capacity for elemental mercury among these three chars, about one order of magnitude lower.

Further insight into the mechanisms for adsorption and the nature of the adsorbing species can be obtained by looking at the adsorption of mercury relative to the char properties. Figure 3-27 shows the results of the first experimental series (3.3 ppmw Hg^0 at 343 K) with the mercury content of the char normalized to the surface area of the char. Thus, if the char surface area is important in determining the capacity for mercury adsorption, the differences between chars seen in Figure 3-26 should be reduced. As Figure 3-27 shows, the surface area does not appear to be correlated with the sorptive capacity of the char.

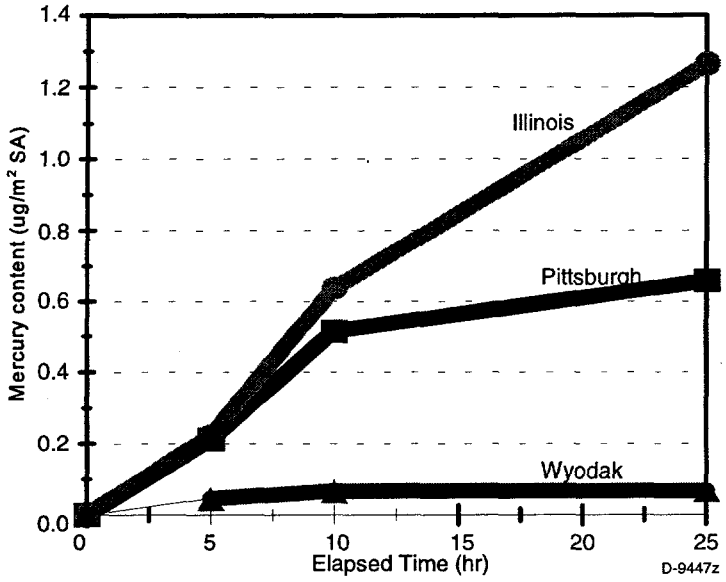

Figure 3-27. Mercury content of chars per square meter of surface area as a function of time for 3.3 ppmw of mercury at a temperature of 343 K.

Surface area of activated carbon is an important physical characteristic that influences adsorption. However, activated carbon is known to be a poor sorbent for elemental mercury. Many previous studies[2-5] have shown additives to activated carbon such as sulfur and iodine can dramatically increase the sorptive capacity of this material for elemental mercury. Therefore, the mercury content has been normalized to the total sulfur content of the chars (Figure 3-28) or to the organic sulfur content of the chars (Figure 3-29). If the sorption curves for the coal chars are coincident, then we could conclude that there is a relationship between the sulfur in the char and the adsorption of elemental mercury. The normalization to total sulfur content (Figure 3-28) brings the Wyodak sorption data closer to that of the bituminous coals, particularly the initial rate. Organic sulfur (Figure 3-29), on the other hand, appears to give excellent agreement between the two bituminous chars, particularly for long times.

By using higher temperatures in the experiment, we could explore higher concentrations as well as the effects of sorbent temperature. There were two source temperature configurations for the high temperature experiment. In one configuration both source and sorbent reaction temperatures were the same: 433 K. In the other configuration the source temperature was 343 K and the reaction temperature (sorbent) is at 433 K. In order to find out the capacity of each of

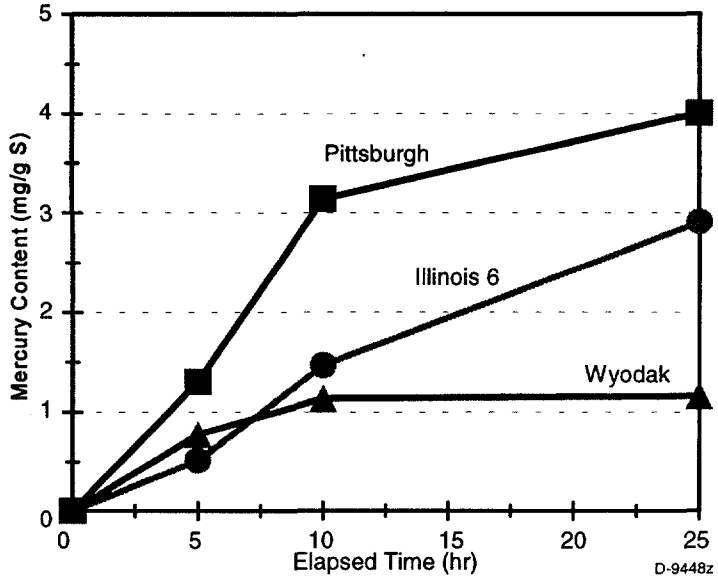

Figure 3-28. Mercury content normalized to total sulfur content as a function of time for chars exposed to simulated flue gas containing 3.3 ppmw Hg^0 at 343 K.

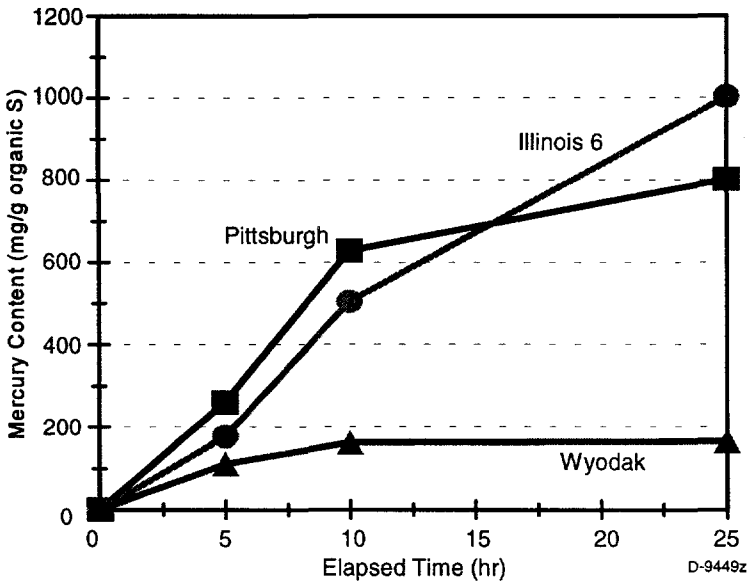

Figure 3-29. Mercury content normalized to organic sulfur content as a function of time for chars exposed to simulated flue gas containing 3.3 ppmw Hg^0 at 343 K.

the coal char in the shortest period, a very high mercury concentration (58 ppmw) experiment was conducted by holding both the source and sorbent at 433 K. Comparing Illinois 6 char with Pittsburgh and Wyodak chars (Figure 3-30), Illinois 6 has a much higher elemental mercury capacity of about 3.2%, followed by Pittsburgh of about 1.54% and Wyodak of 0.26%.

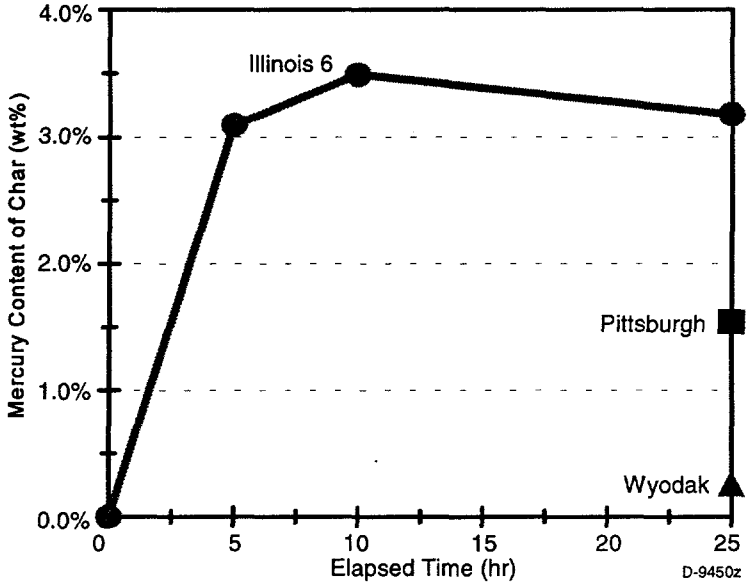

Figure 3-30. Mercury content as a function of time for chars exposed to simulated flue gas containing 58 ppmw Hg^0 at 433 K.

Figure 3-31 illustrates that the results, when normalized to the total sulfur content of the char, provide good agreement for the bituminous chars, although only the Illinois 6 char mercury content was measured at intermediate times. The "final" capacity at 25 hours is 8 mg Hg/g S for the bituminous chars, while for the Wyodak char the capacity is 3 mg Hg/g S.

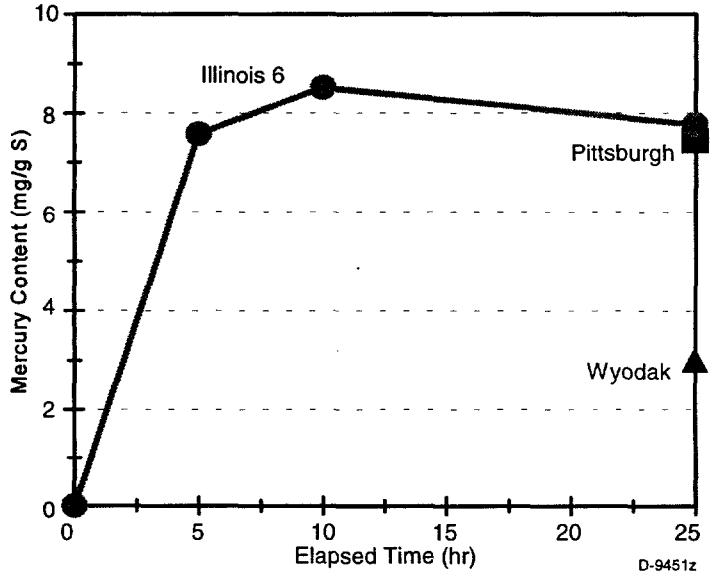

Figure 3-31. Mercury content normalized to total sulfur content as a function of time for chars exposed to simulated flue gas containing 58 ppmw Hg^0 at 433 K.

To look at the effectiveness of the chars as sorbents, it is useful to look at the utilization of sulfur in the high concentration experiments where the char appears to be saturated with mercury. The data at 433 K can be compared to the stoichiometric reaction Hg + S -> HgS as in Figure 3-32. Also in this figure, data on the capacity of activated carbon doped with sulfur are shown. The data of Otani et al.[5] were obtained at a lower temperature (309 K) and at lower mercury concentrations in the gas phase (approximately 6 ppmw in air). Nonetheless, the sulfur utilization is very similar.

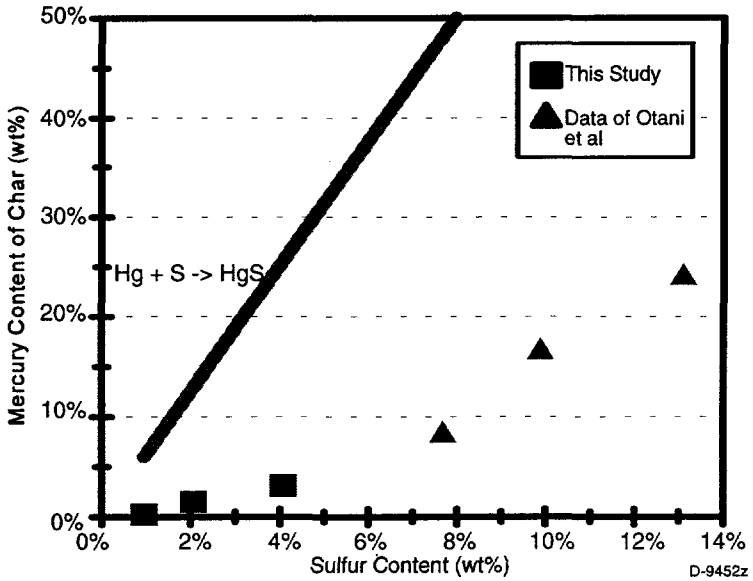

Figure 3-32. Saturated mercury content of chars as a function of total sulfur content. Data of Otani et al. shown for comparison.

Figure 3-33 gives experimental results done under the conditions of 433 K reaction temperature and 343 K source temperature. Temperature control in this system is more critical in order to prevent potential condensation of mercury along the reaction system. Because of the rapid vaporization in the low temperature bath (water vaporization), longer duration experiment, such as 25 hours, was virtually impossible. Therefore only experiments with 5 and 10 hours of duration were performed. Similar performance to the 343 K experiment at low concentration (Figure 3-26) was observed. However the rate of adsorption appears to be lower.

Mercury chloride experiments were somewhat complicated due to the problems in delivering a quantifiable mercury chloride source. Traditionally, a solution injection method has been used to deliver a known concentration of mercury chloride. Because of our special system configuration, this method was not feasible. After an unsuccessful calibration at 343 K temperature (possibly due to the adsorption and reaction of mercury chloride with water), a decision was made to run experiments at high reaction and source temperatures, 433 K, which led to very high mercury chloride concentration. The results are given in Figure 3-34. All three chars showed very high adsorption capacity for mercury chloride; after 5 hours the mercury content of the Illinois 6 char was almost 5%, while the concentration was 4.25% for the

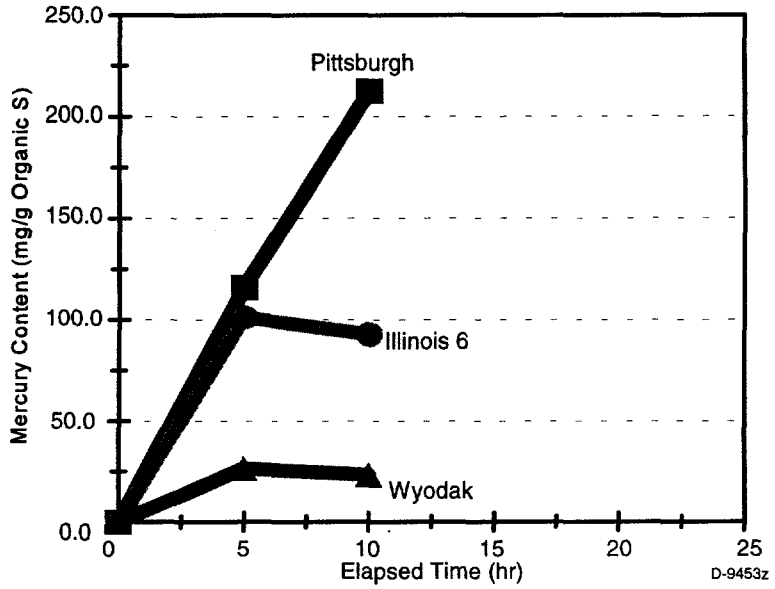

Figure 3-33. Mercury content normalized to organic sulfur content as a function of time for chars exposed to simulated flue gas containing 1.5 ppmw Hg^0 at 433 K.

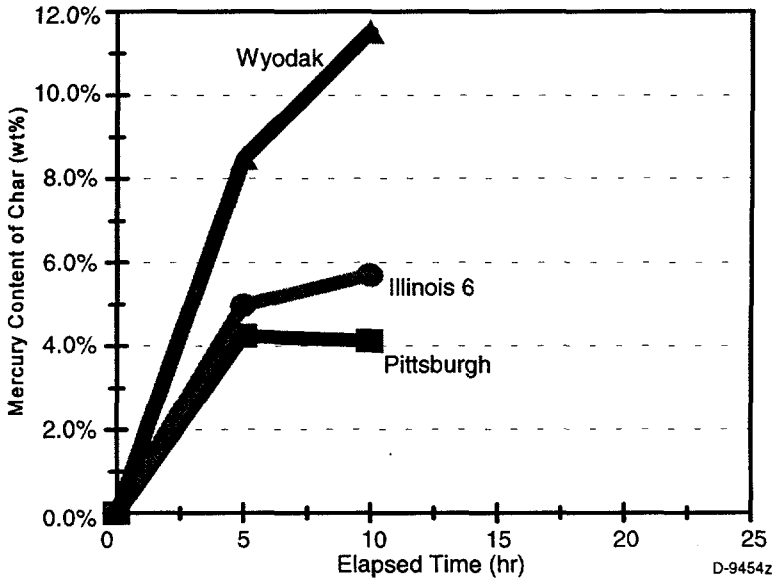

Figure 3-34. Mercury content as a function of time for chars exposed to simulated flue gas containing 61.4 ppmw $HgCl_2$ at 433 K.

Pittsburgh and 8.49% for Wyodak, respectively. The Wyodak has an increase in capacity for $HgCl_2$ of about 50 times as compared with elemental mercury, while the bituminous chars have about twice the sorption capacity for $HgCl_2$ as compared to elemental mercury.

Figure 3-35 shows that the mercury sorption capacity of char is not well correlated with the organic sulfur content for all three chars. When the mercury content of the chars is normalized with respect to the surface area, however, as shown in Figure 3-36, a better correlation is evident, particularly for the initial rate of sorption. The better correlation with surface area for adsorption of mercury chloride points to a physical sorption mechanism, as opposed to a chemical mechanism indicated for elemental mercury.

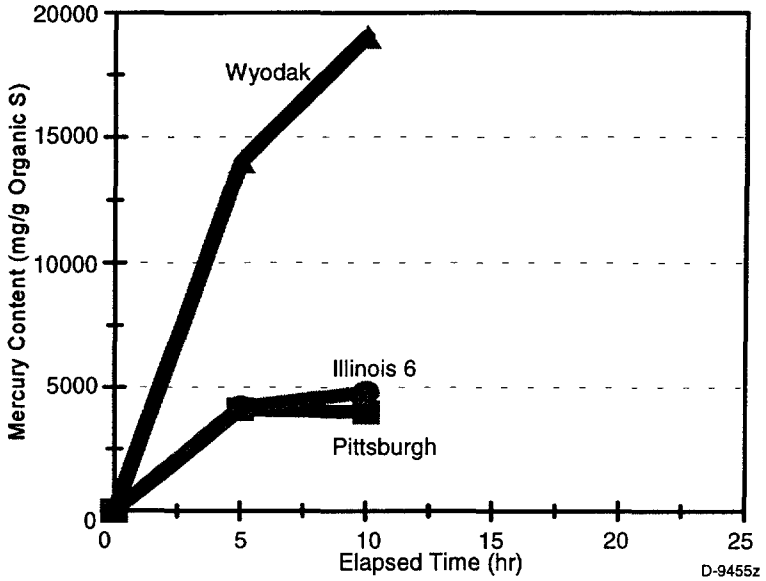

Figure 3-35. Mercury content normalized to organic sulfur content as a function of time for chars exposed to simulated flue gas containing 61.4 ppmw $HgCl_2$ at 433 K.

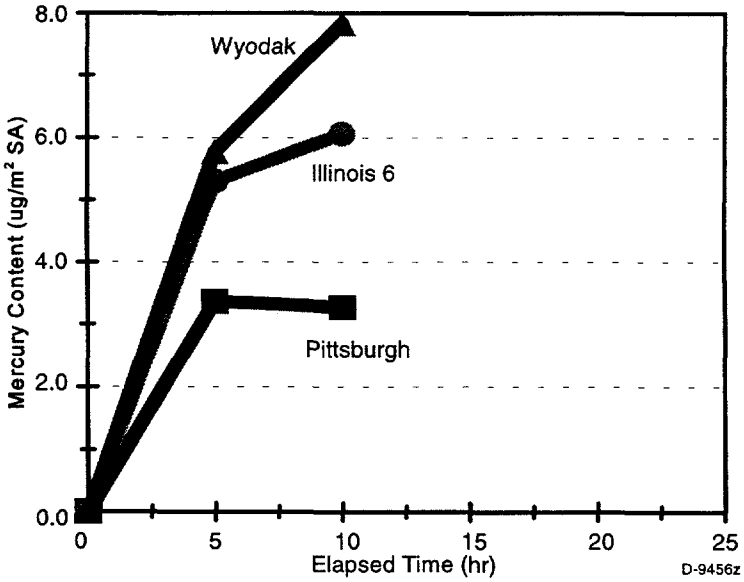

Figure 3-36. Mercury content normalized to char surface area as a function of time for chars exposed to simulated flue gas containing 61.4 ppmw $HgCl_2$ at 433 K.

As discussed in the previous section, there were clear differences in the form of mercury on the char samples based on analysis of XAFS data. With $HgCl_{2(g)}$ as the mercury source, all chars showed an IPD value indicative of Hg_xCl_2 (x=1,2). The experimental data indicate that $HgCl_2$ was adsorbed via a physical adsorption process which is consistent with the XAFS analysis. The Wyodak chars exposed to elemental mercury had IPD values indicative of an Hg-S bond, while the bituminous chars had IPD values in between Hg-S and Hg-Cl. We speculate that a mercury compound containing chlorine and sulfur may form. Thus, formation of a sulfur compound is indicated from the XAFS data when elemental mercury is in the gas phase. This conclusion is supported by the experimental data.

Based on the experimental work, it can be concluded that all three chars, Illinois 6, Pittsburgh and Wyodak, have some degree of elemental mercury and mercury chloride adsorption capacity. For adsorption of elemental mercury, the sulfur utilization of the chars is similar to that for sulfur-doped activated carbon. Higher temperature reduces the initial reaction rate, and has an inverse relationship with the overall mercury adsorption.

These three chars show consistently higher mercury capture in the case of mercury chloride (over elemental mercury) as the mercury source. Elemental mercury appears to react chemically with sulfur in the char, particularly organic sulfur. For mercury chloride, a physical adsorption process seems to be indicated based on the correlation with char surface area. Thus, $HgCl_2$ does not appear to be reacting with sulfur in the char. The organic sulfur content of the char appears to be the better predictor of the affinity of the char for elemental mercury, while the char surface area appears to be the better indicator of affinity of the char for mercuric chloride. XAFS analyses of the chars support these conclusions. In Phase II, we will need to look at the effects of other flue gas constituents on mercury adsorption on coal chars.

3.5 Model Development (PSI)

3.5.1 *Overview*

The objective of the modeling task is to develop a fundamentally-based predictive model to allow utility operators to predict trace element emissions from their plants. The ToPEM will be applicable to *all* combustion conditions including new fuels and coal blends, low-NO_x combustion systems, and new power generation plants. Development of ToPEM will be based on PSI's existing EMAF.

The existing program (EMAF) consists of the following blocks, see also Figure 3-37:

(1) Data reading
(2) A--Generation of coal particles at various sizes with a particle size distribution similar to the input
B--Generation of mineral particles and formation of included and excluded
(3) A-- Distribution of mineral particles to coal particles
B--Combustion of coal particles
C--Formation of ash particles assuming a certain degree of coalescence.

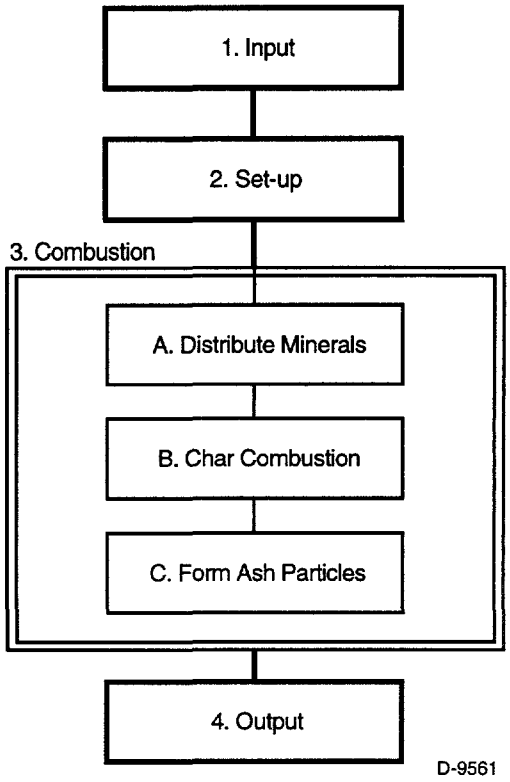

Figure 3-37. Flow chart for Engineering Model for Ash Formation.

As a first step in developing the ToPEM, we will add a sub- model that calculates the evaporation of major elements (Na, K, Fe, Si, Al, Ca and Mg) from both inherent and extraneous minerals of coal.

3.5.2 *Vaporization of Major Elements During Combustion*

Previous work on vaporization of inorganic elements during single particle combustion in the DTF was done by Quann[6] and Quann and Sarofim.[7] This work was both experimental and theoretical. The effects of coal rank, particle size, particle temperature and oxygen concentration were examined. Also, a theoretical analysis on vaporization from included, excluded and atomically dispersed minerals was accomplished. This analysis indicates that the element vaporization depends on one or more of the following parameters: bulk oxygen concentration, coal rank, coal type, particle size and composition of inherent ash. Results of this effort for Si, Ca and Mg were in very good agreement with the experiments.

For the case where we have vaporization from both internal inclusions and exposed inclusion on the char surface (See Figure 3-38), Quann gives:

$$N_{t_0} = N_I^0 \, 4 \pi c \, r_i \, t_b \left[\frac{2}{5} D_e \, x_m^e + \frac{3}{5} D_m \, x_m^{es} \right] \qquad (1)$$

and:

$$N_I^0 = \theta \frac{r_0^3}{r_i^3} \qquad (2)$$

where:

N_{tb} = is the moles of metal vaporized per gram coal burned
N_I^0 = number of inclusions in the char particle
c = molar concentration
r_i = inclusion radius
r_0 = char radius
t_b = burnout time
D_e = effective diffusivity
D_m = metal diffusivity
x_m^3 = equilibrium mole fraction metal at internal inclusion surface
x_m^{es} = equilibrium mole fraction metal at surface of exposed inclusion
θ = volume ratio of inclusions.

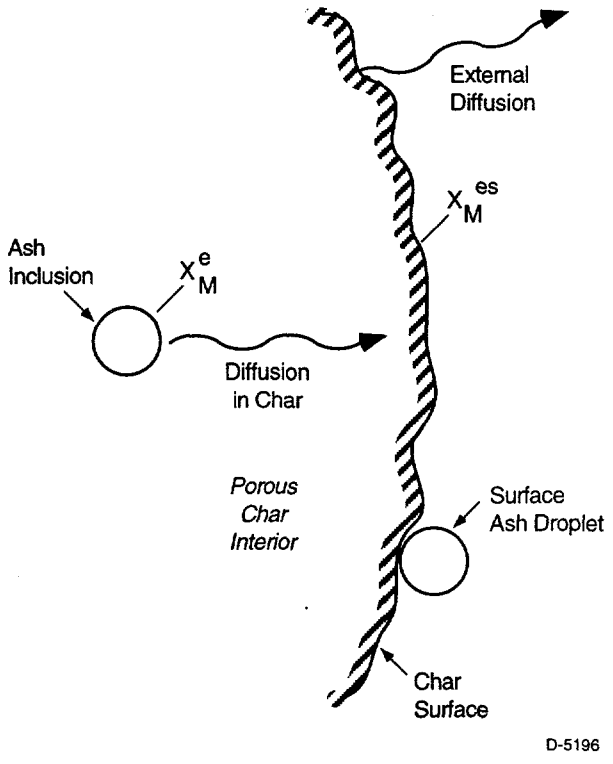

Figure 3-38. Schematic of trace element vaporization mechanisms.

Based on these equations, Mims et al.,[8] derived an expression for the fractional vaporization, f_v, divided by the burnout time, t_B:

$$\frac{f_v}{t_b} = \frac{9\,\pi\,\theta\,c}{r_i^2\,C_o\,\rho_p}\left[\frac{r_i\,D_e\,x_m^e}{2\,r_o\,(3\theta)^{1/2}} + \frac{D_m x_m^{es}}{5}\right] \tag{3}$$

where C_o is the concentration of the metal in the coal and ρ_p is the density of the char particle. For vaporization from the external particles we assume $D_e << D_m$ then:

$$\frac{f_v}{t_b} \sim \frac{1}{r_i^2} \tag{4}$$

This indicates that the parameter is *independent* of char radius.

For the case where internal diffusion is limiting, the effective diffusivity term in Eq. (3) is much higher than the metal diffusion term. Thus:

$$\frac{f_v}{t_b} \sim \frac{1}{r_o} \tag{5}$$

For external diffusion control, as would occur with very fine inclusions or organically associated elements, we have:[8]

$$\frac{f_v}{t_b} = \frac{4\,D_m\,c\,x_m^e}{C_o\,r_o^2} \tag{6}$$

Thus, when external diffusion is controlling we would expect to see a $1/r_o^2$ dependence.

For this work, instead of calculating f_v/t_B from first principles, we used existing experimental results as reference, as described in Ref. 9. The reference data were values for the fractional vaporization of a metal, $(fv/tb)_r$, the equilibrium mole fraction of the metal, x_{ir}, and the coal particle radius (or diameter), r_{or} (d_{or}) for one bituminous and one low rank coal. The reference combustion conditions were a gas temperature of 1750 K and a bulk oxygen partial pressure of 0.2. The particle temperature under such combustion conditions was measured to be 2100K[6,7]. The following equations that use reference data were derived from Eqs. (3), (5) and (6):

$$f_v/t_B = (f_v/t_B)_r (x_i/x_{ir})(r_{or}/r_o) \quad (7)$$

for mineral particles and

$$f_v/t_B = (f_v/t_B)_r (x_i/x_{ir})(r_{or}/r_o)^2 \quad (8)$$

for organically-bound elements.

Note that for Eqs. (7) and (8) we assumed that the metal concentration, C_o, and the volume metal inclusions, θ, were independent of the coal type.

The fraction of a certain element that vaporizes can be calculated if an expression for the burnout time, t_B, is known. This expression was obtained experimentally by Quann:

$$t_B \sim d_o^2/\ln(1+ x_{O2}) \quad (9)$$

where x_{O2} is the molar fraction of oxygen in the combustion gases. This expression is essentially the D^2-Law, which describes the diffusion controlled combustion of particles and droplets.

Using Eq. (9), Eqs. (7) and (8) become:

$$f_v = f_{vr}(x_i/x_{ir})(r_o/r_{or})(1+x_{O_2})/(1+x_{O_2r}) \quad (10)$$

for mineral particles and

$$f_v = f_{vr}(x_i/x_{ir})(1+x_{O_2})/(1+x_{O_2r}) \quad (11)$$

for organically-bound elements.

Equation (10) suggests that for discrete inclusions the fraction of the metal that vaporizes, f_v, is proportional to the particle radius (or diameter), r_o (or d_o). Equation (11) suggests that for atomically dispersed metals f_v is independent of the particle size.

To improve the accuracy of Eqs. (10) and (11) we consider the effect of the metal concentration in coals. According to Eq. (3), the fraction of the metal that vaporizes, f_v, is inversely proportional to the metal concentration in the coal, C_o. This effect can be taken into account by multiplying the right hand side of Eqs. (7) and (8) (or Eqs. (10) and (11)) by C_{or}/C_o, where the subscript *r* refers to the reference coal. In the calculations that follow, the effect of the metal concentration in the coal was initially omitted and subsequently was taken into account for all metals.

Experimental results from Quann indicate that the amount of magnesium that vaporizes varies linearly with the magnesium content of coal. Therefore, the fraction of magnesium that vaporizes is independent of the magnesium content of coal. Indeed, the assumption that the vaporization of magnesium is independent of the coal concentration in magnesium improved the accuracy of the calculations, as seen in the next section.

The metal gaseous mole fractions, x_i and x_{ir}, are calculated by assuming that the metal oxides undergo reduction during evaporation, for example:

$$SiO_{2©} + CO <=> SiO + CO_2$$

And the partial pressure of SiO is equal to:

$$P_{SiO} = (a_{SiO_2} K_{eq} P_{CO})^{1/2}$$

where a_{SiO2} is the activity coefficient and K_{eq} is the equilibrium constant. The activity coefficient is assumed to be independent of coal type and combustion conditions, so it cancels out in Eqs. (7) and (8) (or (10) and (11)). The equilibrium constants used were curvefits from JANAF data over a temperature range of 1500 to 2500 K as shown in Table 3-13.[9]

Table 3-13. Equilibrium Constants for Vaporization of Metals

$\ln(K) = a + 10^4 b/T$	a	b
$SiO_{2(l)} + CO <=> SiO + CO_2$	18.6621	-5.9507
$Al_2O_{3(l)} + CO <=> 2AlO + CO_2$	38.2805	-16.7937
$FeO_{(l)} + CO <=> Fe + CO_2$	11.0258	-4.2495
$CaO_{(l)} + CO <=> Ca + CO_2$	10.1895	-5.1918
$MgO_{(l)} + CO <=> Mg + CO_2$	11.8032	-4.5773
$Na_2O_{(l)} + CO <=> 2Na + CO_2$	17.7349	-2.8271
$K_2O_{(l)} + CO <=> 2K + CO_2$	19.1685	-2.1940

The simple equilibria between CO and CO_2 can be used for each metal species of interest, assuming that oxygen diffusing to the char particle surface is completely consumed and that CO is the only product of combustion. In this case, the bulk oxygen concentration, P_{O2b}, will determine the concentration of CO at the surface:

$$P_{COs} = 2\, P_{O2b}/(1 + P_{O2b})$$

The bulk oxygen concentration can be calculated by assuming that all the volatiles burn first.

Comparison with Experimental Results

Equations (10) and (11) were used to predict metal vaporization and composition of the resulting submicron ash for a variety of coals, coal particles sizes and oxygen concentrations. All coals were analyzed and burned by Quann, who obtained experimental data for metal vaporization and composition of submicron ash. The calculations were then compared to the experimental data. Predictions were made for vaporization of SiO_2, Na_2O, K_2O, CaO, FeO, SiO_2, Al_2O_3 and MgO. The amount of oxides vaporized was summed to get a calculated value of the total ash vaporized. Results of this effort are given in the Appendix (Tables A-1 to A-7) and in Figures 3-39 to 3-51.

As reference values for Eqs. (10) and (11), the following experimental data we used: (a) for vaporization of Na, Si and Al from bituminous coals, we used data for Illinois 6 from Quann,[6,7] (b) for vaporization of Na, Si, Al, Ca and Mg from sub-bituminous coals and lignites, we used data for Montana Savage lignite from Quann,[6,7] (c) for vaporization of Fe we used correlations from data of Ref. 10, and (d) for vaporization of K we used the following correlation from Ref. 9:

$$f_K = 0.007706 + 0.615746 * f_{Na} \qquad (12)$$

Vaporization of major elements was predicted for Illinois 6 at four different cases (Figures 3-39 and 3-40): (a) 50 μm particles burning at 1750 K and 20% O_2, (b) 120 μm particles burning at 1750 K and 20% O_2, (c) 50 μm particles burning at 1750 K and 40% O_2, and (d) 120 μm particles burning at 1750 K and 40% O_2.

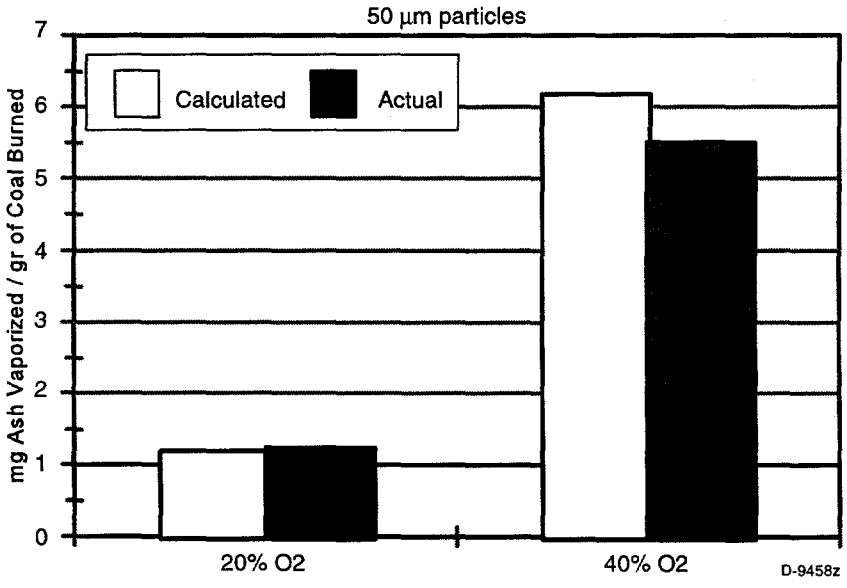

Figure 3-39. Effect of oxygen concentration on ash vaporization from Illinois 6. Particles burning at 1750 K, 20% and 40% oxygen. Particle diameter is 50 μm.

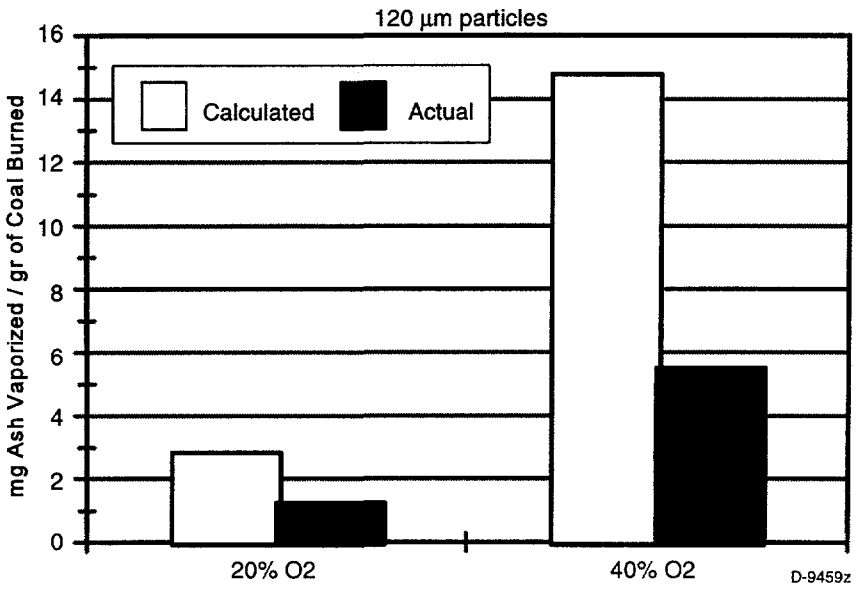

Figure 3-40. Effect of oxygen concentration on ash vaporization from Illinois 6. Particles burning at 1750 K, 20% and 40% oxygen. Particle diameter is 120 µm.

The calculations predict within 12% the total amount of ash that vaporizes from combustion of 50 µm particles at 20% and 40% oxygen. The predicted submicron ash composition for these cases is generally good. However, the evaporation of K is substantially overpredicted and the evaporation of Si underpredicted. The calculations overpredict the amount of ash that evaporates from 120 µm particles by two or three times.

Figure 3-41 displays predicted and actual values for ash vaporization from three bituminous coals, Illinois 6, Alabama Rosa and Pittsburgh. The combustion conditions were 1750 K and 20% oxygen. The coal particle size was 60 µm. The ash content of these coals is in the range of 6.6 to 13.7 % and the extraneous mineral content is in the range of 16 to 56%. The inherent ash composition is similar in all these coals, with the exception of CaO in Pittsburgh, which has 2.5 to 3.5 times as much CaO as the other coals. The element concentration in the coal was accounted for in these calculations by multiplying the right hand size of Eqs. (7) and (8) by C_{or}/C_o. The combustion conditions were 1750 K and 20% oxygen.

The amount of ash that vaporizes from Alabama Rosa is predicted now more accurately (within 9%) than previously (within 55%, see Table A-2). The amount of ash that vaporizes from the Pittsburgh coal is predicted to be the same in both sets of calculations. The predicted ash composition, see Figures 3-42 to 3-44, is better than that presented in Table A-2.

Figures 3-45 and 3-46 as well as Table A-4 contain calculated and actual values for Montana Savage Lignite at four different cases: (a) 60 µm particles burned at 1750 K and 20% O_2, (b) 120 µm particles burned at 1750 K and 20% O_2, (c) 60 µm particles burned at 1750 K and 40% O_2, and (d) 120 µm particles burned at 1750 K and 40% O_2.

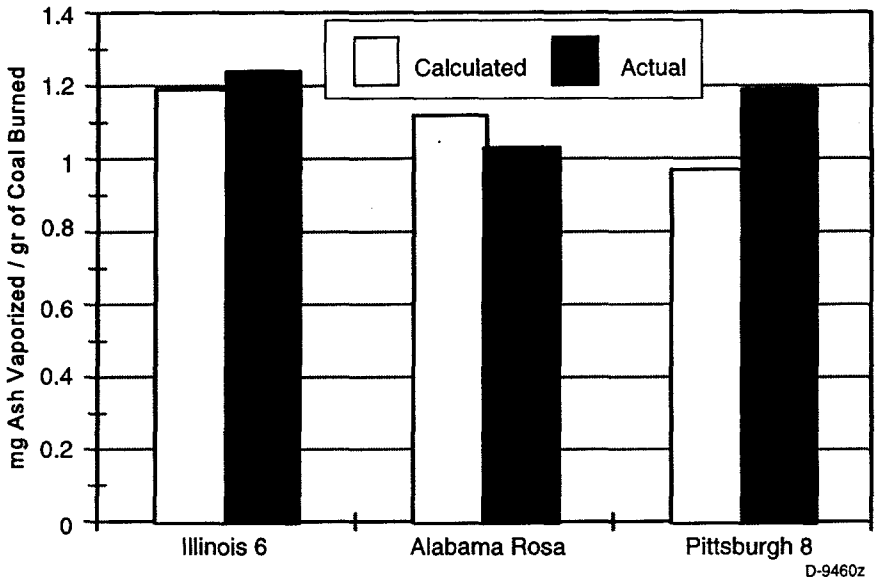

Figure 3-41. Effect of coal type on ash vaporization from bituminous coals. Particles burning at 1750 K and 20% oxygen. Particle diameter is 50 μm.

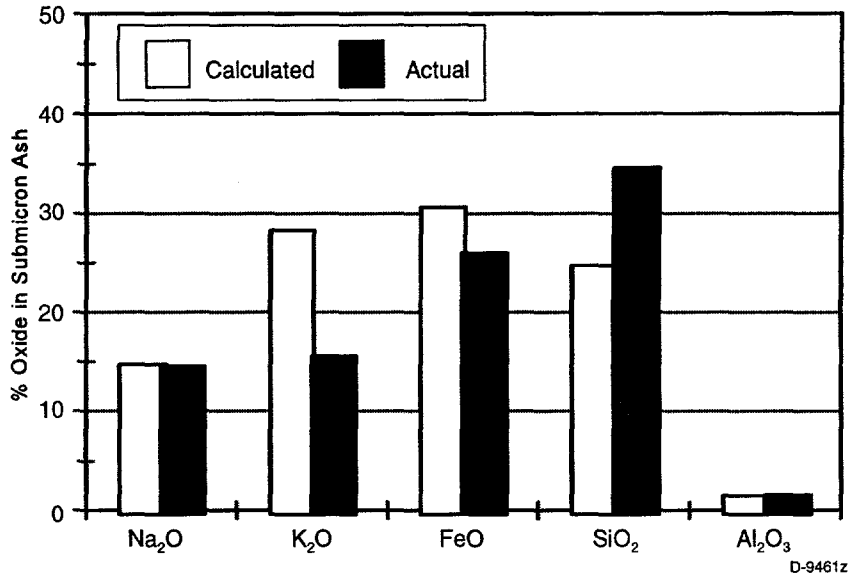

Figure 3-42. Submicron ash composition from Illinois 65. Particles burning at 1750 K and 20% oxygen. Particle diameter is 50 μm.

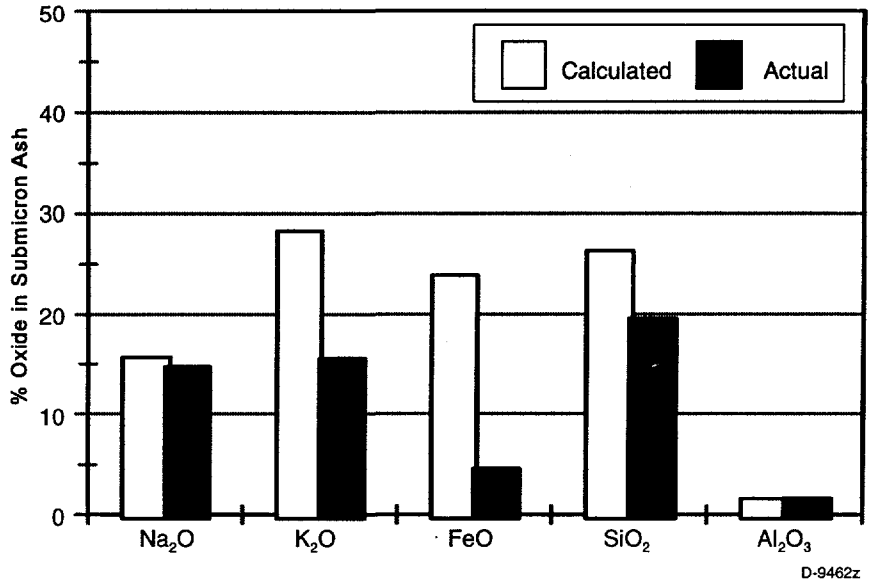

Figure 3-43. Submicron ash composition from Alabama Rosa. Particles burning at 1750 K and 20% oxygen. Particle diameter is 50 μm.

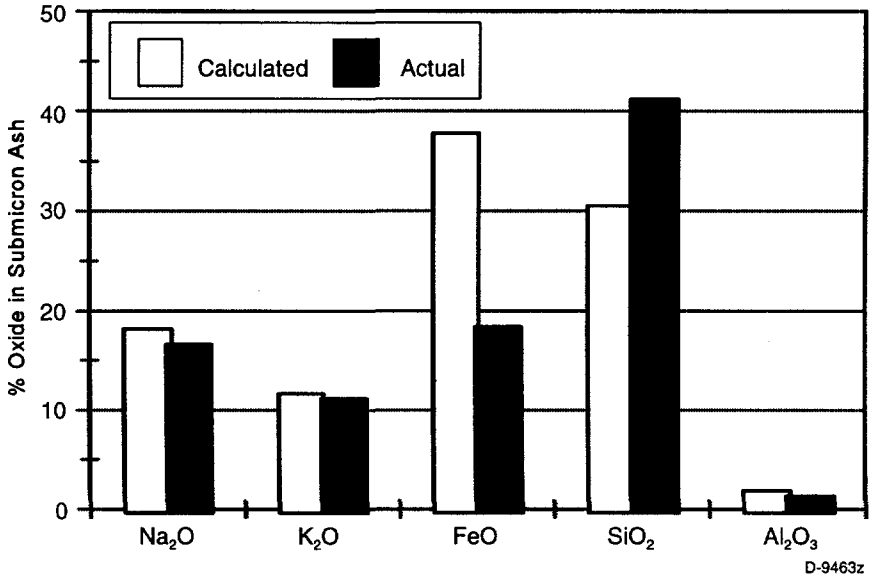

Figure 3-44. Submicron ash composition from Pittsburgh coal. Particles burning at 1750 K and 20% oxygen. Particle diameter is 50 μm.

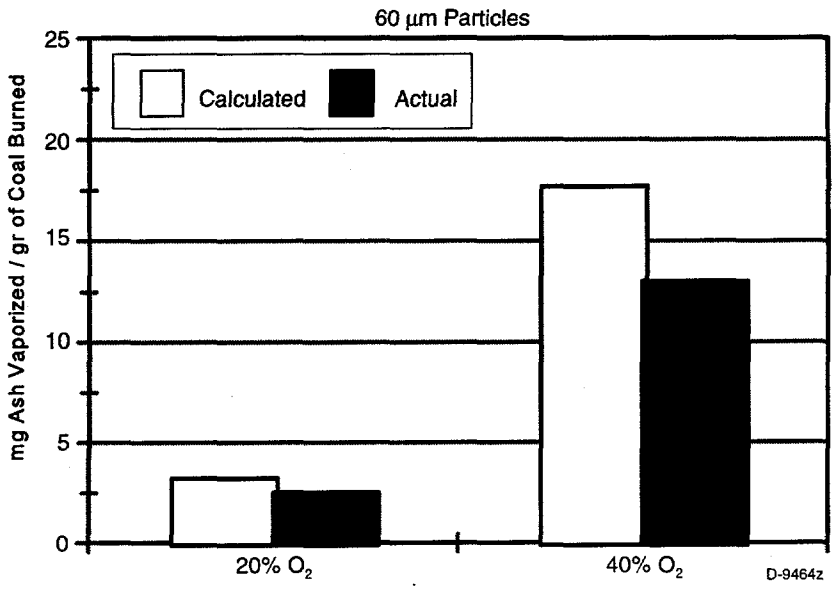

Figure 3-45. Effect of oxygen concentration on ash vaporization from Montana Savage lignite. Particles burning at 1750 K, 20% and 40% oxygen. Particle diameter is 60 µm.

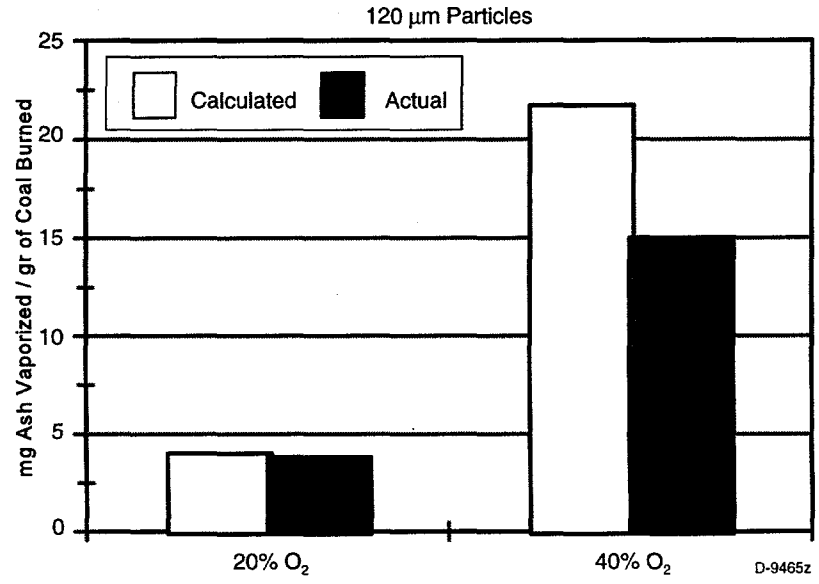

Figure 3-46. Effect of oxygen concentration on ash vaporization from Montana Savage lignite. Particles burning at 1750 K, 20% and 40% oxygen. Particle diameter is 120 µm.

These calculations predict within 26% and 5% the total amount of ash that vaporizes from combustion of 60 and 120 μm particles, respectively, at 20% oxygen. The calculated submicron ash composition agrees well with the experimental data. The calculations at 40% oxygen concentrations overpredict the amount of ash that evaporates by 46 to 53%.

Figure 3-47 and Table A-5 contain predicted and actual values for ash vaporization from four low rank coals, Montana Savage lignite, Montana Rosebud sub-bituminous, Montana Powder River Basin (PRB) sub-bituminous and N. Dakota lignite. The combustion conditions were 1750 K and 20% oxygen. The coal particle size was 60 μm. The ash content of these coals is in the range of 7.5 to 13.6 % and extraneous mineral content is in the range of 14 to 64% of the total ash content. The inherent ash composition varied substantially between these coals. As an example Na_2O in the inherent ash varied in the range of 0.41 for Montana PRB to 16.44% for N. Dakota lignite. The amount of ash that vaporizes is predicted within 50%.

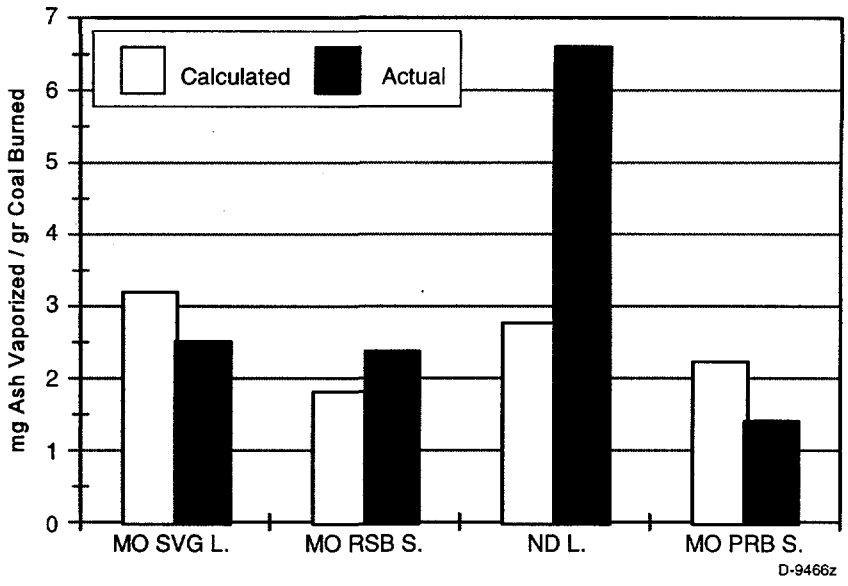

Figure 3-47. Effect of coal type on ash vaporization from low rank coals. Particles burning at 1750 K and 20% oxygen. Particle diameter is 60 μm.

Table A-6 contains predicted and actual values for ash vaporization from the same three low rank coals presented at Table A-5. Results in the former table were calculated by taking into account the element concentration in the coal for all these metals. Comparing the results of Tables A-5 and A-6, the latter table shows predictions for the composition of the sub-micron ash that are more accurate than those presented in the former. The accuracy of the absolute amount of the ash that vaporizes is similar in both cases.

Finally, another improvement to the model was made. Quann's experimental results suggest that there is a linear relationship between the inherent magnesium in coal and the amount of magnesium that vaporizes. Therefore, the fraction of magnesium that vaporizes is constant and independent of the inherent magnesium in coal. The effect of metal concentration was taken into account for all metals except the magnesium. Results of these calculations for four low rank coals are shown in Figures 3-47 to 3-51 as well as Table A-7. It can be seen that both the predicted amount of ash that vaporizes and the predicted ash composition have improved substantially with the exception of N. Dakota Lignite, see Figure 3-50. The ash vaporization of N. Dakota Lignite, which has extremely high Na content, is better predicted assuming that the metal vaporization does not depend on the metal concentration in the coal.

3.5.3 *Summary*

This work aimed to develop a model that predicts the vaporization of metals during coal combustion. The model is based on other existing models, experimental data and correlations of data. The main factors that affect the metal vaporization are: the coal rank, the coal type, the coal particle size, the oxygen content (and therefore the particle temperature) and the metal concentration in the coal.

Bituminous Coals

Our model predicts fairly accurately the amount of ash that vaporizes and the submicron ash composition of bituminous coals based on a fixed reference condition. The effect of oxygen concentration and the metal composition of the coal on the ash vaporization are predicted well, but the effect of the coal particle diameter is not predicted accurately. Experimental results

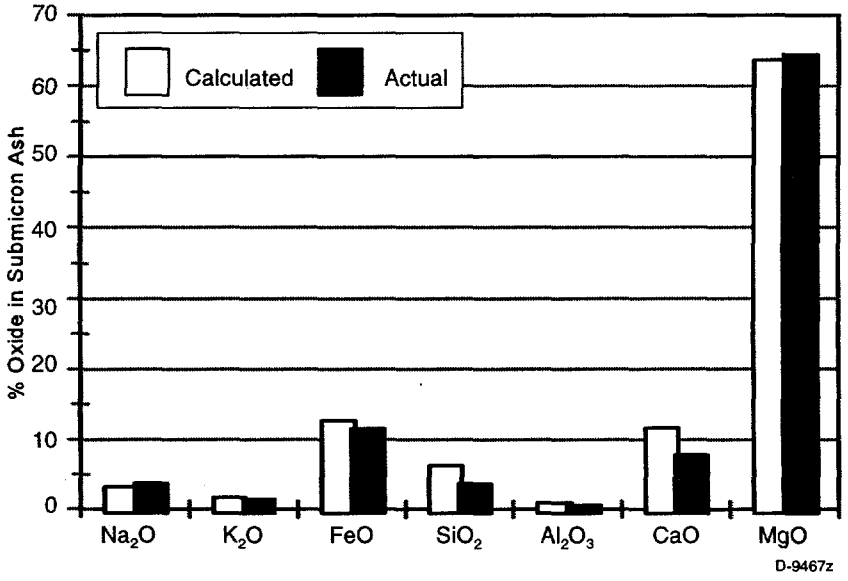

Figure 3-48. Submicron ash composition from Montana Savage lignite. Particles burning at 1750 K and 20% oxygen. Particle diameter is 60 μm.

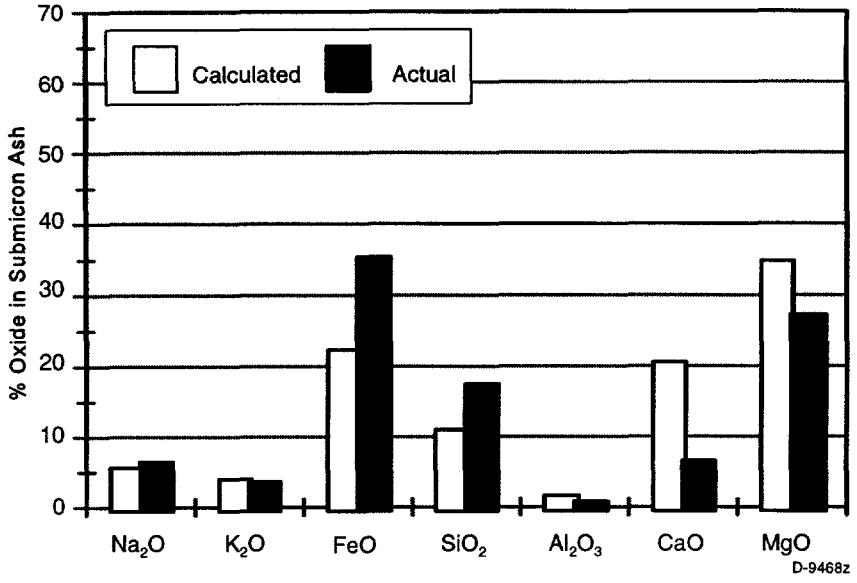

Figure 3-49. Submicron ash composition from Montana Rosebud sub-bituminous. Particles burning at 1750 K and 20% oxygen. Particle diameter is 60 μm.

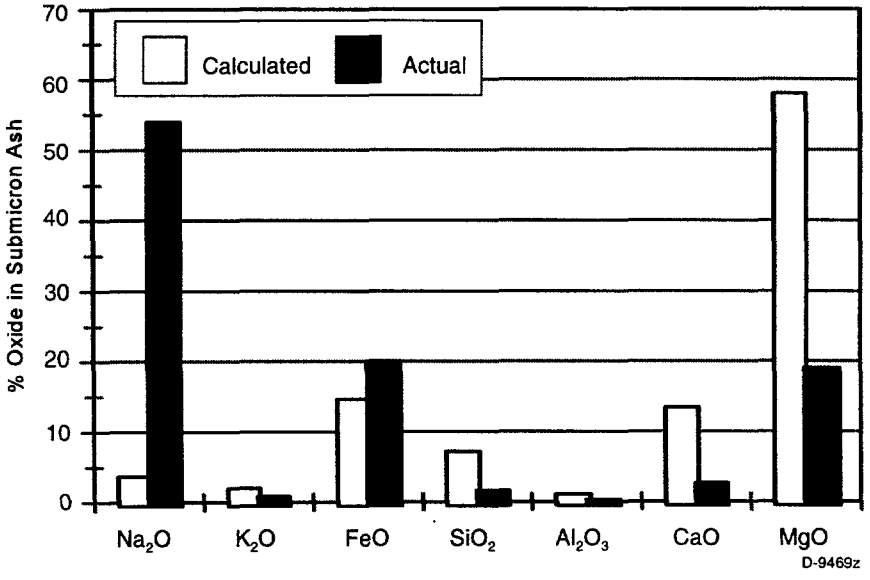

Figure 3-50. Submicron ash composition from N. Dakota lignite particles burning at 1750 K and 20% oxygen. Particle diameter is 60 μm.

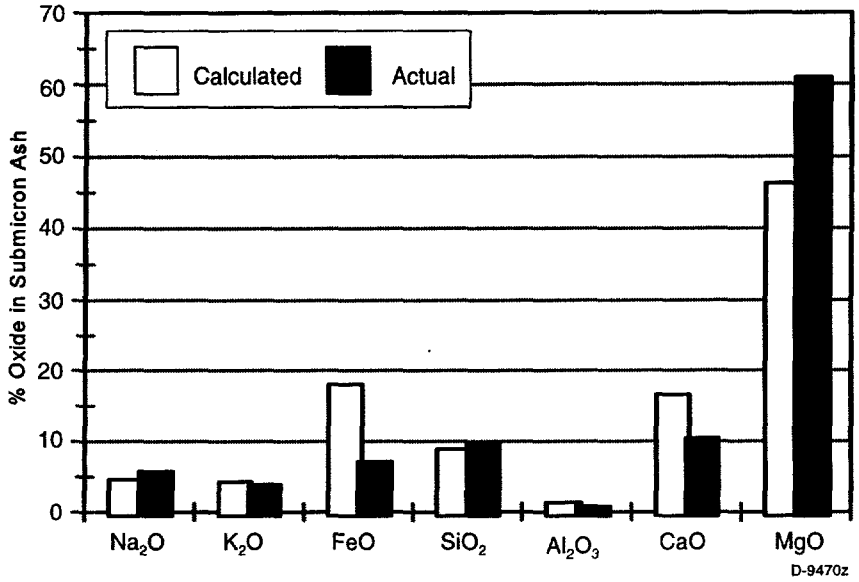

Figure 3-51. Submicron ash composition from Montana PRB sub-bituminous particles burning at 1750 K and 20% oxygen. Particle diameter is 60 μm.

suggest that metal vaporization for bituminous coals is independent of coal particle size, while our model predicts a linear relationship. The modeling efforts should concentrate in the following areas: (a) the effect of coal particle size on the element evaporation, and (b) the accuracy of potassium, iron, and silicon vaporization predictions.

Low Rank Coals

Our model predicts fairly accurately the amounts of ash that vaporizes and the submicron ash composition from a variety of low rank coals based on a fixed reference condition. The model predicts the effect of coal particle size on the ash vaporization better than it does the effect of oxygen concentration, unlike the case of the bituminous coals. The modeling efforts should concentrate on the following areas: (a) the effects of coal particle size and oxygen concentration on the element evaporation, and (b) the accuracy of calcium vaporization predictions.

SECTION 4

SUMMARY

4. SUMMARY

In the reporting period through June, 1998 the Phase II program was begun. Three coals were selected for detailed study in Phase II: an Ohio bituminous coal, a Wyodak seam Powder River Basin sub-bituminous coal, and a North Dakota lignite. Samples of all three coals were procured. Pulverized samples of two of the coals (Ohio and North Dakota) were distributed to team members. Analytical work on the pulverized samples was started.

Analysis of data taken in the Phase I program continued during the reporting period. Experiments were carried out on the volatility of trace elements during heating of the coals. Relatively slow heating in air (consistent with ASTM ashing procedure, for example) did not produce a significant loss of trace elements in coal samples. However, rapid heating (consistent with the ASTM procedure for determination of volatile matter) resulted in significant loss of trace elements. Further investigations will be undertaken in Phase II to determine if this latter procedure can provide any information on the forms of trace elements in coal samples.

Mass balance closure calculations were made for the combustion experiments at MIT's Drop Tube Furnace (DTF) and PSI's Entrained Flow Reactor (EFR). In the pyrolysis experiments at MIT, Na and Se showed poor mass balance closure, while in combustion experiments, Na, Cr, Co, and Sb showed poor mass balance closure. The PSI combustion experiments showed low mass balance closure for Br, As, Se, and Sb. These elements which exhibited poor mass balance closure are either volatile at combustion temperatures or organically associated. Care must be taken in the Phase II combustion experiments at Utah to obtain good mass balance closure for trace elements.

Additional statistical analysis of Phase I data was performed to investigate mechanistic information related to the fate of the radionuclides Cs, Th, and Co during the combustion of Pittsburgh seam coal and Illinois #6 coal at the University of Arizona. Condensation via heterogeneous reaction appears to be the dominant transformation mechanism in the post-combustion zone for all three elements when burning either coal. There was correlation between ash particle Ca concentration and the concentration of Cs and Th when burning Pittsburgh coal, suggesting formation of a calcium-radionuclide complex in the ash. This was not observed for the Illinois coal, nor for Co in either coal. Analytical methods were developed to analyze trace metals using graphite furnace atomic spectroscopy (GFAA). These methods were applied to additional Phase I impactor data to determine the concentration of As in Pittsburgh fly ash samples.

During the course of this project (Phase I through the present), we have accumulated much XAFS data on mercury in various sorbents and on a wide range of Hg compounds. Almost without exception, the first features that occur on the mercury absorption edge are two inflection points, whose positions and intensities appear to be related to chemical bonding differences. In particular, the separation of these inflection points appears to correlate with differences in the ionicity of the Hg-NN bond. The more ionic compounds of mercury, such as HgO, mercury sulfate, etc., in which the Hg ion is surrounded by oxygen anions, have large values for the separation of the inflection points, whereas the least ionic species such as Hg iodides and diphenyl mercury have small separations. The data for this inflection point difference (IPD) were

assembled for thirteen pure mercury compounds. These IPD values were compared to those from previously measured mercury sorbent samples. Many of the UA IPD values are compatible with chloride and/or sulfide as the coordinating ligand around mercury. Other sorbent samples obtained from PSI showed values are outside the chloride/sulfide range. For several zeolite samples the values were higher, whereas several activated carbon samples had lower values. The IPD values for the zeolite sorbents were compatible with oxidic species, such as the sulfate species. The activated carbon samples, however, may indicate that the principal bonding was between Hg and C, as the IPD values are closest to that of diphenyl mercury. Much work remains to be done in Phase II to determine the limits of confidence of the IPD values, but the method of analysis has the potential for pinpointing specific mercury species on solid samples.

Analysis of the vapor phase mercury-char experiments was modified this period to incorporate new XAFS data on forms of sulfur in the char samples. The basic conclusion remained the same: Elemental mercury appears to react chemically with sulfur in the char, particularly organic sulfur, while for mercury chloride, a physical adsorption process seems to be indicated. The IPD values for the chars, as determined by UK, support this conclusion.

During this period development was begun on a submodel that predicts the vaporization of major metals during coal combustion. The model is based on other existing models, experimental data and correlations of data. The main factors that affect the metal vaporization are: the coal rank, the coal type, the coal particle size, the oxygen content (and therefore the particle temperature) and the metal concentration in the coal. Our model predicts fairly accurately the amounts of ash that vaporize and the submicron ash composition from a variety of bituminous coals. The effect of oxygen concentration and the metal composition of the coal on the ash vaporization are predicted well, but the effect of the coal particle diameter is not predicted accurately. Our model predicts fairly accurately the amounts of ash that vaporize and the submicron ash composition from a variety of low rank coals. Coal particle size had a pronounced effect on the ash vaporization, unlike the case of the bituminous coals.

During the next quarter (July through September, 1998), the rest of the coal samples will be distributed to team members. Standard analyses will be completed for the program coals and advanced analyses will be under way. Preparations will be made for combustion experiments at UC, UU, and UA. Model development work on ash vaporization and submicron aerosol formation will continue.

SECTION 5

REFERENCES

5. REFERENCES

1. Huffman, G.P.,. Mitra, S., . Huggins, F.E., and Shah, N., *Energy & Fuels*, **1991**, *5*, p. 574-581.

2. Dunham, G.E. and Miller, S.J. "Evaluation of Activated Carbon for Control of Mercury from Coal-Fired Boilers" presented at the First Joint Power and Fuel Systems Contractors Conference, July 9-11, 1996, Pittsburgh, PA.

3. Krishnan, S.V., Gullett, B.K., and Jozewicz, W. "Sorption of Elemental Mercury by Activated Carbon" *Env.Sci.Tech.* **1994**, *28*, 1506-1512.

4. Vidic, R.D. and McLaughlin, J.B. "Uptake of Elemental Mercury Vapors by Activated Carbons" *J.Air Waste Manage.Assoc.* **1996**, *46*, 241-250.

5. Otani, Y., Emi, H., Kanoaka, I., and Nishiro, H., "Removal of Mercury Vapor from Air with Sulfur-Impregnated Adsorbents," *Env.Sci.Tech.* **1988**, *22*, 708-711.

6. Quann, R.J., Sc.D. Thesis, Department of Chemical Engineering, MIT, Cambridge, MA (1982).

7. Quann, R.J. and Sarofim, A. F. , "Vaporization of Refractory Oxides During Purverized Coal Combustion". Nineteenth (International) Symposium on Combustion, The Combustion Institute, 1982, pp. 1429-1440.

8. Mims, C.A., Neville, M., Quann, R.J. and Sarofim, A.F. "Laboratory Studies of Trace Element Transformations During Coal Combustion." Presented at 87th AIChE Meeting, Boston, MA 1979.

9. Bool, II, L.E., Heble, J.J. Shah, N., Shah, A., Huffman, G.P., Huggins, F.E., Rao, K.R.P.M., Sarofim, A.F., Zeng, T. , Reschke, R., Gallien, D. and Peterson, T.W. " Fundamental Study of Ash Formation and Deposition: Effect of Reducing Stoichiometry," Final Report prepared for Department of Energy, PETC, under Contract No. DE-AC22-93PC92190, PSIT-1178/TR-1407, September 1995.

10. Senior, C.L., Bool, II, Morency, J., Huggins, F., Huffman, G.P., Shah, N., Wendt, J.O.L., Shadman, F., Peterson, T.W., Seams, W., Wu, B., Sarofim, A.F., Olmez, I., Zeng, T., Crowley, S., Kolker, A., Palmer, C.A., Finkelman, R., Heble, J.J., and Wornat, M.J., "Toxic Substances from Coal Combustion- A Comprehensive Assessment." Final Report prepared for Department of Energy, PETC, under Contract No. DE-AC22-95PC95101, PSI-1245/TR-1505, September 1997.

APPENDIX

PREDICTED AND MEASURED VAPORIZATION OF MAJOR ELEMENTS DURING COAL COMBUSTION

Table A-1. Illinois 6 Effect of Particle Size and Oxygen Concentration on Metal Vaporization

TR-1178 fv/tb=(fv/tb)r* xi/sr*Dr/D	**x=0.2, 50 µm 1750 K - calc. (Measured)**		**x=0.4, 50 µm 1750 K - calc. (Measured)**		**x=0.2, 120 µm 1750 K - calc. (Measured)**		**x=0.4, 120 µm 1750 K - calc. (Measured)**	
mg ash ev/g coal	1.19	(1.24)	6.18	(5.5)	2.84	(1.24)	14.77	(5.5)
% ash coal vap.	0.87	(0.90)	4.54	(5)	2.09	(0.90)	10.86	(5)
% Na_2O, subash	14.70	(14.5)	4.093		14.88		4.10	
µg Na v/gr coal	130	(155)	186	(160)	310	(230)	452	(280)
% K_2O, subash	28.30	(15.6)	6.865		27.77		6.433	
µg K v/gr coal	280	(116)	350		274		783	
% FeO, subash	30.64	(26.0)	27.02		30.90		27.11	
µg Fe v/gr coal	280	(180)			690	(180)		
% SiO_2 subash	24.73	(34.6)	41.40		24.94		41.55	
µg Si v/gr coal	137	(202)					2860	(202)
% Al_2O_3, subash	1.50	(1.6)	2.06		14.98		2.06	

Table A-2. Bituminous Coals
Effect of Coal Type on Metal Vaporization

Metal Concentration of Coal is Accounted for
Combustion Conditions: 1750 K and x=0.2, Coal Particle Size 50 µm

TR-1178 fv/tb=(fv/tb)r* xi/xr*Dr/D	**Illinois 6 Calculated (Measured)**		**Alabama Rosa Calculated (Measured)**		**Pittsburgh Calculated (Measured)**	
mg ash ev/g coal	1.19	(1.24)	0.46	(1.03)	0.97	(1.19)
% ash coal vap.	0.87	(0.90)	0.70	(1.56)	1.32	(1.63)
% Na_2O, subash	14.70	(14.5)	16.96	(14.71)	26.19	(16.64)
% K_2O, subash	28.30	(15.6)	26.39	(4.60)	16.48	(11.20)
% FeO, subash	30.64	(26.0)	31.35	(47.40)	33.92	(18.40)
% SiO_2, subash	24.73	(34.6)	23.45	(19.60)	21.63	(41.20)
% Al_2O_3, subash	1.50	(1.6)	1.84	(1.60)	1.76	(1.31)
Note: Alabama Rosa has the highest amount of extraneous minerals of all bituminous coals						

Table A-3. Bituminous Coals
Effect of Coal Type on Metal Vaporization

Metal Concentration of Coal is Not Accounted for
Combustion Conditions: 1750 K and x=0.2, Coal Particle Size 50 μm

TR-1178 fv/tb=(fv/tb)r* xi/xr*Dr/D*Cor/Co	**Illinois 6 Calculated (Measured)**		**Alabama Rosa Calculated (Measured)**		**Pittsburgh Calculated (Measured)**	
mg ash ev/g coal	1.19	(1.24)	1.12	(1.03)	0.97	(1.19)
% ash coal vap.	0.87	(0.90)	1.71	(1.56)	1.32	(1.63)
% Na_2O, subash	14.7	(14.5)	15.69	(14.71)	18.20	(16.64)
% K_2O, subash	28.3	(15.6)	23.85	(4.60)	11.67	(11.20)
% FeO, subash	30.64	(26.0)	32.57	(47.40)	37.78	(18.40)
% SiO_2, subash	24.73	(34.6)	26.29	(19.60)	30.50	(41.20)
% Al_2O_3, subash	1.50	(1.6)	1.58	(1.60)	1.83	(1.31

Table A-4. Montana Lignite
Effect of Particle Size and Oxygen Concentration on Metal Vaporization

TR-1178 fv/tb=(fv/tb)r* xi/xr*Dr/D	**x=0.2, 60 µm 1750 K - calc. (Measured)**		**x=0.4, 60 µm 1750 K - calc. (Measured)**		**x=0.2, 120 µm 1750 K - calc. (Measured)**		**x=0.4, 120 µm 1750 K - calc. (Measured)**	
mg ash ev/g coal	3.19	(2.51)	17.66	(13)	3.98	(3.8)	21.70	(15)
% ash coal vap.	3.63	(2.86)	20.07	(11.0)	4.52	(3.0)	24.66	(15.0)
% Na_2O, subash	3.20	(3.7)	0.83		5.14		1.35	
% K_2O, subash	1.67	(1.4)	0.37		2.64		0.58	
% FeO, subash µg Fe ug/gr coal	12.68 315	(11.5) (185)	8.03		20.34		6.54	
% SiO_2 subash µg Si v/gr coal	6.20 (93)	(3.67) (40)	9.75		10.00		15.87	
% Al_2O_3, subash µg Al v/gr coal	0.92	(0.56)	11.90		1.47		19.41	
% CaO, subash µg Ca v/gr coal	11.66 534	(7.8) (135)	13.24		9.35		10.78	
MgO, subash µg Mg v/gr coal	63.62 (1733)	(64.40)	55.84		51.05		45.45	

Table A-5. Sub-Bituminous Coals and Lignites
Effect of Coal Type on Metal Vaporization

Metal Concentration of Coal is Not Accounted for
Combustion Conditions: 1750 K and x=0.2, Coal Particle Size 60 μm

TR-1178 fv/tb=(fv/tb)r* xi/xr*Dr/D*C/Cr	**Montana Savage Lignite Calculated (Measured)**		**Montana Rosebud Sub. Calculated (Measured)**		**N. Dakota Lignite Calculated (Measured)**		**Montana PRB sub. Calculated (Measured)**	
mg ash ev/g coal	3.4	(2.51)	2.62	(2.38)	8.10	(6.60)	2.87	(1.41)
% ash coal vap.	3.85	(2.86)	1.93	(1.74)	10.80	(8.85)	2.31	(1.13)
% Na_2O, subash	3.03	(3.70)	3.95	(6.5)	42.76	(54.00)	3.85	(5.70)
% K_2O, subash	1.58	(1.40)	2.84	(3.6)	10.47	(0.82)	3.48	(3.80)
% FeO, subash	11.93	(11.50)	47.15	(35.4)	19.20	(20.00)	24.33	(7.10)
% SiO_2, subash	5.90	(3.67)	9.45	(17.5)	2.16	(1.62)	18.81	(9.90)
% Al_2O_3, subash	0.87	(0.56)	0.85	(0.80)	0.24	(0.27)	1.52	(0.78)
% CaO, subash	16.67	(7.80)	11.64	(6.60)	5.3	(2.65)	12.06	(10.40)
MgO, subash	59.90	(64.40)	23.97	(27.20)	19.85	(19.00)	35.99	(61.00)

Table A-6. Sub-Bituminous Coals and Lignites
Effect of Coal Type on Metal Vaporization

Metal Concentration of Coal is Accounted for
Combustion Conditions: 1750 K and x=0.2, Coal Particle Size 60 μm

TR-1178 fv/tb=(fv/tb)r* xi/xr*Dr/D*C/Cr	**Montana Savage Lignite Calculated (Measured)**		**Montana Rosebud Sub. Calculated (Measured)**		**N. Dakota Lignite Calculated (Measured)**		**Montana PRB sub. Calculated (Measured)**	
mg ash ev/g coal	3.4	(2.51)	3.43	(2.38)	3.40	(6.6)	3.32	(1.41)
% ash coal vap.	3.85	(2.86)	2.74	(1.74)	4.52	(8.85)	2.58	(1.13)
% Na_2O, subash	3.03	(3.70)	3.00	(6.5)	3.03	(54.00)	3.16	(5.70)
% K_2O, subash	1.58	(1.40)	2.76	(3.6)	1.63	(0.82)	2.92	(3.80)
% FeO, subash	11.93	(11.50)	11.79	(35.4)	11.93	(20.00)	12.5	(7.10)
% SiO_2, subash	5.90	(3.67)	5.84	(17.5)	5.90	(1.62)	6.51	(9.90)
% Al_2O_3, subash	0.87	(0.56)	0.86	(0.80)	0.87	(0.27)	0.90	(0.78)
% CaO, subash	16.67	(7.80)	16.56	(6.60)	16.75	(2.65)	11.51	(10.40)
MgO, subash	59.90	(64.40)	59.18	(27.20)	59.87	(19.00)	62.81	(61.00)

Table A-7. Sub-Bituminous Coals and Lignites
Effect of Coal Type on Metal Vaporization

Metal Concentration of Coal is Accounted for, except for Magnesium
Combustion Conditions: 1750 K and x=0.2, Coal Particle Size 60 μm

TR-1178 fv/tb=(fv/tb)r* xi/xr*Dr/D*C/Cr	**Montana Savage Lignite Calculated (Measured)**		**Montana Rosebud Sub. Calculated (Measured)**		**N. Dakota Lignite Calculated (Measured)**		**Montana PRB sub. Calculated (Measured)**	
mg ash ev/g coal	3.20	(2.51)	1.81	(2.38)	2.77	(6.60)	2.23	(1.41)
% ash coal vap.	3.63	(2.86)	1.33	(1.74)	3.69	(8.85)	1.79	(1.13)
% Na_2O, subash	3.20	(3.70)	5.64	(6.5)	3.69	(54.00)	4.57	(5.70)
% K_2O, subash	1.67	(1.40)	4.05	(3.6)	2.00	(0.82)	4.21	(3.80)
% FeO, subash	12.68	(11.50)	22.35	(35.4)	14.60	(20.00)	18.09	(7.10)
% SiO_2, subash	6.23	(3.67)	11.00	(17.5)	7.18	(1.62)	8.90	(9.90)
% Al_2O_3, subash	0.92	(0.56)	1.62	(0.80)	1.06	(0.27)	1.31	(0.78)
% CaO, subash	11.66	(7.80)	20.55	(6.60)	13.43	(2.65)	16.63	(10.40)
MgO, subash	63.62	(64.40)	34.76	(27.20)	58.02	(19.00)	46.26	(61.00)